

การค้นพบและศึกษาระบบดาวคู่หลังผิวห่อหุ้มร่วม : SDSS

J074548.63+263123.4



นายนิวัฒน์ เหมหา

วิทยานิพนธ์นี้เป็นส่วนหนึ่งของการศึกษาตามหลักสูตรปริญญาวิทยาศาสตรมหาบัณฑิต

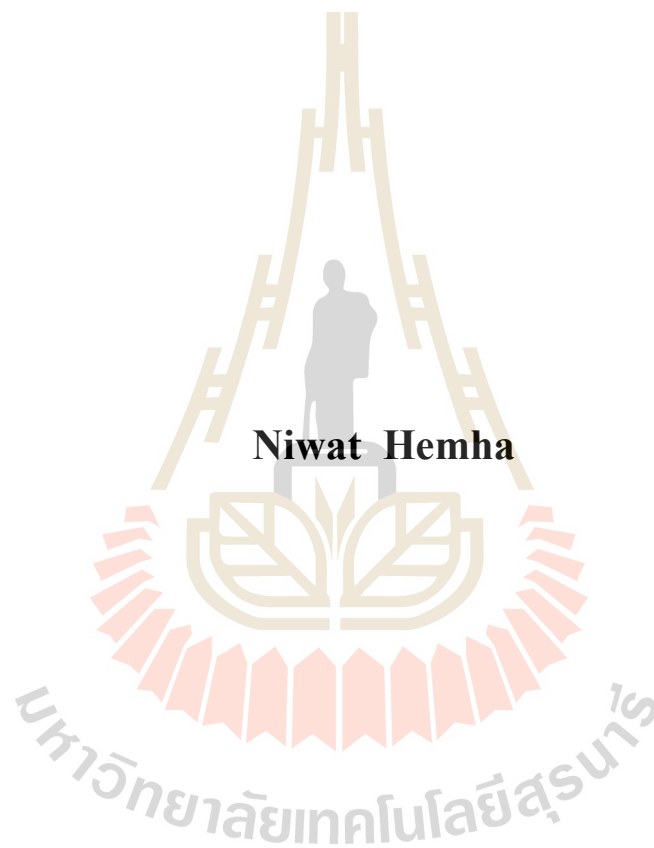
สาขาวิชาฟิสิกส์

มหาวิทยาลัยเทคโนโลยีสุรนารี

ปีการศึกษา 2559

**DISCOVERY AND STUDY OF ECLIPSING POST
COMMON-ENVELOPE SYSTEM :**

SDSS J074548.63+263123.4



**A Thesis Submitted in Partial Fulfillment of the Requirements for the
Degree of Master of Science in Physics
Suranaree University of Technology
Academic Year 2016**

DISCOVERY AND STUDY OF ECLIPSING POST COMMON

ENVELOPE SYSTEM : SDSS J074548.63+263123.4

Suranaree University of Technology has approved this thesis submitted in partial fulfillment of the requirements for a Master's Degree.

Thesis Examining Committee



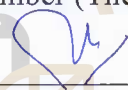
(Asst. Prof. Dr. Worawat Meevasana)

Chairperson



(Dr. Nuanwan Sanguansak)

Member (Thesis Advisor)



(Dr. Puji Irawati)

Member



(Asst. Prof. Dr. Amornrat Aungwerojwit)

Member



(Prof. Dr. Santi Maensiri)

Acting Vice Rector for Academic
Affairs and Internationalisation



(Prof. Dr. Santi Maensiri)

Dean of Institute of Science

นิวัฒน์ เหมหา : การค้นพบและศึกษาระบบดาวคู่หลังพัวห่อหุ้มร่วม : SDSS J074548.63
+263123.4 (DISCOVERY AND STUDY OF ECLIPSING POST COMMON
ENVELOPE SYSTEM : SDSS J074548.63+263123.4) อาจารย์ที่ปรึกษา : อาจารย์ ดร.
นवलวรรณ สงวนศักดิ์, 81 หน้า.

วิทยานิพนธ์ฉบับนี้จัดทำขึ้นเพื่อศึกษาระบบดาวคู่ SDSS J0745 +2631 ซึ่งผู้วิจัยได้ทำการสังเกตการณ์ระบบดาวนี้ครั้งแรกเมื่อวันที่ 7 มกราคม 2557 โดยใช้กล้องโทรทรรศน์ขนาดเส้นผ่านศูนย์กลาง 2.4 เมตร ร่วมกับ ULTRASPEC โดยใช้แผ่นกรองแสง g' r' และ KG5 ตามลำดับ ซึ่งจากการวิเคราะห์ข้อมูล SDSS J0745 +2631 พบว่าเป็นระบบดาวคู่อุปราคา และสามารถสังเกตช่วงอุปราคาได้ชัดเจนที่สุดโดยใช้แผ่นกรองแสง g' แต่สำหรับแผ่นกรองแสง r' นั้นไม่สามารถเห็นอุปราคาได้อย่างชัดเจน เนื่องจากในช่วงความยาวคลื่นสีแดงนั้นกราฟแสงนั้นได้รับอิทธิพลจากดาวในแถบลำดับหลัก ซึ่งแสดงให้เห็นลักษณะการส่ายอย่างมากแบบ ellipsoidal และความไม่สมมาตรของกราฟแสงระหว่างช่วงเฟส 0.5 และ 1.0 ของการโคจร จากการจำลองระบบดาวคู่นี้ด้วยโปรแกรม Binary Maker 3.0 และ JKTEBOP พบว่าดาวเคราะห์ขาวมีอุณหภูมิยังผล 14594 ± 217 K และมีรัศมี 0.008 ± 0.002 เท่าของรัศมีดวงอาทิตย์ ส่วนดาวในแถบลำดับหลักมีอุณหภูมิยังผล 3750 ± 250 K และมีรัศมี 0.427 ± 0.006 เท่าของรัศมีดวงอาทิตย์ และมีขนาดของดาวเกือบเต็มพัวห่อหุ้มของโรซ นอกจากนี้ยังพบว่าอัตราส่วนของมวลระหว่างดาวในแถบลำดับหลักกับดาวเคราะห์ขาวคือ 0.37 ± 0.01 และมีคาบการโคจร 0.21926 ± 0.00005 วัน

สาขาวิชาฟิสิกส์

ปีการศึกษา 2559

ลายมือชื่อนักศึกษา นิวัฒน์ เหมหา

ลายมือชื่ออาจารย์ที่ปรึกษา นवलวรรณ สงวนศักดิ์

ลายมือชื่ออาจารย์ที่ปรึกษาร่วม

NIWAT HEMHA : DISCOVERY AND STUDY OF ECLIPSING POST

COMMON ENVELOPE SYSTEM : SDSS J074548.63+263123.4

THESIS ADVISOR : NUANWAN SANGUANSUK, Ph.D. 81 PP.

ECLIPSING BINARY SYSTEM/ULTRASPEC/ELLIPSOIDAL MODULATION

In this work, SDSS J0745+2631 was investigated. The first observation was obtained on 7th January 2014 using the 2.4-meter Thai National Telescope (TNT) with ULTRASPEC using filter g' , r' and KG5. SDSS J0745+2631 is classified as an eclipsing binary system which the eclipse was clearly seen in the filter g' light curve. The feature of the main-sequence star is more dominating in the filter r' . The light curve shows a large ellipsoidal modulation and asymmetry between orbital phases 0.5 to 1.0. The models of the binary system are obtained by using Binary Maker 3.0 and JKTEBOP codes. The white dwarf has an effective temperature of 14594 ± 217 K and radius $0.008 \pm 0.002R_{\odot}$. For the main-sequence star, the effective temperature is 3750 ± 250 K, its radius is $0.427 \pm 0.006R_{\odot}$ and almost fills its Roche lobe. The mass ratio (M_2/M_1) of the system is 0.37 ± 0.01 with an orbital period of 0.21926 ± 0.00005 days.

School of Physics

Academic Year 2016

Student's Signature

Niwat Hemha

Advisor's Signature

N. Sanguansuk

Co-advisor's Signature

ACKNOWLEDGEMENTS

I am grateful to my thesis supervisors, Dr. Nuanwan Sanguansak and Dr. Puji Irawati for their help and kindness for this work. Before I decided to do the research about the binary star I had a talk with Dr. Nuanwan Sanguansak about astronomy field studying. During my master degree studying, I had an opportunity from Dr. Nuanwan Sanguansak to know Dr. Puji Irawati my co-advisor, they encouraged me to study astronomy and pay a lot of attention to my work especially, the correction of my thesis. Without them, my thesis could not be finished.

I would also like to acknowledge NARIT and the operation team that helped and supported during my observation and did the research at NARIT, Science Achievement Scholarship of Thailand (SAST) for the scholarship since my bachelor degree and a partially support from the Center of Excellence in High Energy Physics and Astrophysics, SUT.

Finally, thank to my parents and friends who always give me the encouragement and support whenever I feel depressed and cheer me up.

Niwat Hemha

CONTENTS

| | Page |
|--|-------------|
| ABSTRACT IN THAI..... | I |
| ABSTRACT IN ENGLISH | II |
| ACKNOWLEDGEMENTS..... | III |
| CONTENTS..... | IV |
| LIST OF TABLE | VIII |
| LIST OF FIGURES | IX |
| CHAPTER | |
| I INTRODUCTION AND REVIEW OF THE LITERATURE | 1 |
| 1.1 Introduction and review of the literature..... | 1 |
| 1.2 Research objective..... | 4 |
| 1.3 Scope and limitations of the study | 4 |
| II THEORY | 6 |
| 2.1 Eclipsing binary..... | 6 |
| 2.1.1 Two body system..... | 6 |
| 2.1.2 The Roche Geometry..... | 8 |
| 2.1.3 Limb darkening and reflection effect | 10 |
| 2.1.4 Gravity darkening..... | 11 |
| 2.1.5 Orbital parameters | 12 |
| 2.1.6 Heliocentric correction | 15 |
| 2.1.7 Orbital period changes in eclipsing binary | 16 |

CONTENTS (Continued)

| | Page |
|---|-------------|
| 2.2 Binary star evolution | 17 |
| 2.2.1 Mass exchange | 19 |
| 2.2.1.1 Conservative mass transfer..... | 20 |
| 2.2.1.2 Non-conservative mass transfer | 20 |
| 2.2.2 The formation of the common-envelope | 21 |
| 2.2.3 The common-envelope phase..... | 21 |
| 2.2.4 Post-Common-Envelope | 22 |
| 2.3 Physical properties of M-type star and White Dwarf..... | 23 |
| 2.3.1 M-type star | 23 |
| 2.3.2 White Dwarf star | 24 |
| III METHODOLOGY | 26 |
| 3.1 Observation | 26 |
| 3.1.1 Target selection..... | 26 |
| 3.1.2 Telescope: Thai National Telescope (TNT)..... | 28 |
| 3.1.3 ULTRASPEC | 29 |
| 3.1.4 Data acquisition system..... | 30 |
| 3.1.5 Filters..... | 30 |
| 3.1.6 Observation data..... | 33 |
| 3.2 Data reduction | 35 |
| 3.2.1 Bias-subtraction..... | 37 |
| 3.2.2 Flat-fielding | 38 |

CONTENTS (Continued)

| | Page |
|--|-----------|
| 3.2.3 The photometry with IRAF | 38 |
| 3.3 Data analysis..... | 39 |
| 3.3.1 Calculation of correction observation time | 39 |
| 3.3.2 Calculation the relative flux | 39 |
| 3.3.3 Calculation of orbital phase..... | 40 |
| 3.4 Light curve modeling | 40 |
| 3.4.1 Binary Maker 3.0..... | 40 |
| 3.4.1.1 Effective temperature of stars..... | 41 |
| 3.4.1.2 Mass ratio of the system..... | 42 |
| 3.4.1.3 Inclination..... | 42 |
| 3.4.1.4 Mass of main-sequence and white dwarf | 42 |
| 3.4.1.5 Orbital separation | 43 |
| 3.4.1.6 Limb darkening | 44 |
| 3.4.1.7 Gravity Darkening Exponent..... | 44 |
| 3.4.1.8 Reflection effect | 45 |
| 3.4.1.9 Stellar spot..... | 45 |
| 3.4.2 JKTEBOP code | 46 |
| IV RESULT AND DISCUSSIONS..... | 51 |
| 4.1 Light curve analysis..... | 51 |
| 4.2 Time of mid-eclipse..... | 51 |
| 4.3 O-C and ephemeris..... | 56 |

CONTENTS (Continued)

| | Page |
|--|-------------|
| 4.4 Light curve fitting..... | 58 |
| 4.4.1 Model with BM 3.0 program of SDSS J0745+2631 | 58 |
| 4.4.2 Model with JKTEBOP code of SDSS J0745+2631 | 61 |
| 4.5 Stellar parameters | 63 |
| 4.6 Discussions | 66 |
| 4.6.1 Eclipse of SDSS J074548.63+263123.4..... | 67 |
| 4.6.2 Large ellipsoidal modulation and inclination | 67 |
| 4.6.3 Stellar parameters of SDSS J074548.63+263123.4 | 71 |
| 4.6.4 Orbital period of SDSS J074548.63+26312.4..... | 72 |
| 4.6.5 Stellar spot on SDSS J0745 +2631..... | 72 |
| 4.6.6 Reflection effect | 73 |
| V CONCLUSIONS AND FUTRE WORK | 74 |
| 5.1 Conclusions | 74 |
| 5.2 Future work | 76 |
| REFERENCES | 77 |
| CURRICULUM VITAE | 81 |

LIST OF TABLES

| Table | Page |
|-------|---|
| 3.1 | ULTRASPEC filters. λ_c is the central wavelength and $\Delta\lambda$ is the FWHM.....35 |
| 3.2 | Photometric observations log of SDSS J0745+263136 |
| 3.3 | Linear Limb Darkening.....44 |
| 3.4 | The initial parameter of JKTEBOP for SDSS J0745+263147 |
| 3.5 | The final parameter of JKTEBOP for SDSS J0745+263149 |
| 4.1 | The observed mid-eclipse from the models by using BM 3.054 |
| 4.2 | The observed mid-eclipse from the output of JKTEBOP code.....55 |
| 4.3 | The predicted mid-eclipse time from calculation55 |
| 4.4 | The $O - C$ calculations57 |
| 4.5 | The reduce Chi square for light curve data by using BM 3.061 |
| 4.6 | The reduce Chi square for light curve data by using JKTEBOP63 |
| 4.7 | Parameters of SDSS J0745+2631 from JKTEBOP63 |
| 4.8 | Parameters of SDSS J0745+2631 from BM 3.064 |
| 5.1 | The stellar and binary parameters of SDSS J0745+263175 |

LIST OF FIGURES

| Figure | Page |
|---|------|
| 1.1 Light curve of SDSS J0745+2631 from Parsons et al. (2013) | 2 |
| 1.2 CSS light curve of SDSS J0745+2631 from Parsons et al. (2013) | 3 |
| 1.3 SDSS spectrum of SDSS J0745+2631 from Parsons et al. (2013) | 3 |
| 1.4 Light curve of SDSS J0745+2631 from Parsons et al. (2015) | 4 |
| 2.1 Co-rotating coordinate for a binary star system | 7 |
| 2.2 Cross section of equipotential surface of a binary system | 9 |
| 2.3 The cross section of star for the limb darkening effect | 10 |
| 2.4 The light curve of PG 1336-018 | 11 |
| 2.5 The geometry of an eclipsing binaries star when the inclination of system i ... | 12 |
| 2.6 The binary star system | 13 |
| 2.7 The light curve of an eclipsing binaries system | 13 |
| 2.8 Light travel time as Earth revolves about the Sun | 16 |
| 2.9 The conservative mass transfer after the first common envelope stage | 18 |
| 2.10 The common envelope stage | 18 |
| 2.11 Schematic of the main evolutionary phases of a PCEBs | 22 |
| 2.12 Hertzsprung-Russell Diagram | 25 |
| 3.1 The visibility chart of SDSS J0745+2631 on 7 th January 2014 | 27 |
| 3.2 Thai National Telescope 2.4-meter and the Thai National Observatory | 28 |
| 3.3 The frame-transfer EMCCD chip mounted in the cryostat | 29 |

LIST OF FIGURES (Continued)

| Figure | Page |
|---|------|
| 3.4 The diagram of the ULTRASPEC EMCCD | 31 |
| 3.5 The diagram of the principal hardware of the ULTRASPEC | 32 |
| 3.6 The filter wheel of the ULTRASPEC | 33 |
| 3.7 The transmission profiles of the ULTRASPEC SDSS filters | 34 |
| 3.8 Flow chart of the data reduction processing | 38 |
| 3.9 The light curves from observing night of 7 th January 2014 | 41 |
| 3.10 The diagram for circular orbits: CM marks the barycenter | 43 |
| 3.11 The light curve of SDSS J0745 +2631 from observation night 7 th January 2014 | 46 |
| 4.1 The light curves of SDSS J0745+2631 after bias subtraction and flat-fielding | 52 |
| 4.2 The light curves in the range of orbital phase 0.9 -1.1 | 53 |
| 4.3 The light curves from observation and from BM 3.0 | 54 |
| 4.4 The $O - C$ diagram which $P = 0.21926$ days and $T_0(\text{HJD}) = 2453387.75524$ | 56 |
| 4.5 BM3 models with and without stellar spot for data obtained on 7 th January 2014 and 20 th December 2014..... | 59 |
| 4.6 BM3 models with and without stellar spot for data obtained on 22 nd December 2014 and 11 th January 2016 | 60 |
| 4.7 JKTEBOP models | 62 |
| 4.8 CSS light curves of SDSS J0750+4943 and SDSS J2229+1853 | 69 |

LIST OF FIGURES (Continued)

| Figure | Page |
|--|------|
| 4.9 A geometry model of SDSS J0745+2631 by using BM 3.0 | 69 |
| 4.10 A surface outline of SDSS J0745+2631 by using BM 3.0..... | 70 |
| 4.11 A Geometry of primary eclipse which change a radii by a change inclination | 70 |



CHAPTER I

INTRODUCTION AND REVIEW OF THE LITERATURE

1.1 Introduction and review of the literature

Binary stars are two stars orbiting around their center of mass. They are classified into four types according to the way in which they are observed: visually, by observation; spectroscopically, by periodic change in spectrum lines; photometrically, by changes in brightness caused by an eclipse; or astrometrically, by measuring a deviation in a star's position caused by an unseen companion (Hilditch, 2001).

In this thesis, the system that we are focusing on is the binary in which one star is a white dwarf star (WD) and the other is a main-sequence star (MS). This new candidate for eclipsing PCEB was discovered by Parsons et al 2013 from Sloan Digital Sky Survey (SDSS) and Catalina Sky Survey (CSS). SDSS J074548.63+263123.4 (or SDSS J0745+2631) was first recognized as a WDMS due to the blue excess in its spectra. The light curve of SDSS J0745+2631 which was observed in r' filter (Figure 1.1) shows a very shallow dip on phase zero making it difficult to recognize the primary eclipse, also SDSS J0745+2631 shows a very large ellipsoidal modulation (almost 0.3 mag) as seen in Figure 1.2, implying that the main-sequence is close to filling its Roche lobe. The spectrum of SDSS J0745+2631 shows that the main-sequence star dominates overall flux at optical wavelengths as presented in Figure 1.3. Hence, the system was not confirmed by Parsons et al. (2013) as eclipsing binary.

The uncertainty of the eclipsing nature of SDSS J0745+2631 is our main motivation to study this binary system. It is also important to determine the physical parameters of this system. SDSS J0745+2631 was observed using the 2.4-meter Thai National Telescope (TNT) with ULTRASPEC in different filters. The light curves of SDSS J0745+2631 were then analyzed using relative photometry method with IRAF. In term of modeling and obtaining the physical parameters of this system, Binary Maker 3.0 (BM 3.0) software and JKTEBOP code were used.

Recently, Parsons et al. (2015) reported their new data of SDSS J0735+2631, which was obtained in g' filter (Figure 1.4). Using this new observation, they confirmed that SDSS J0745+2631 is an eclipsing system, which is in agreement with our independent observation.

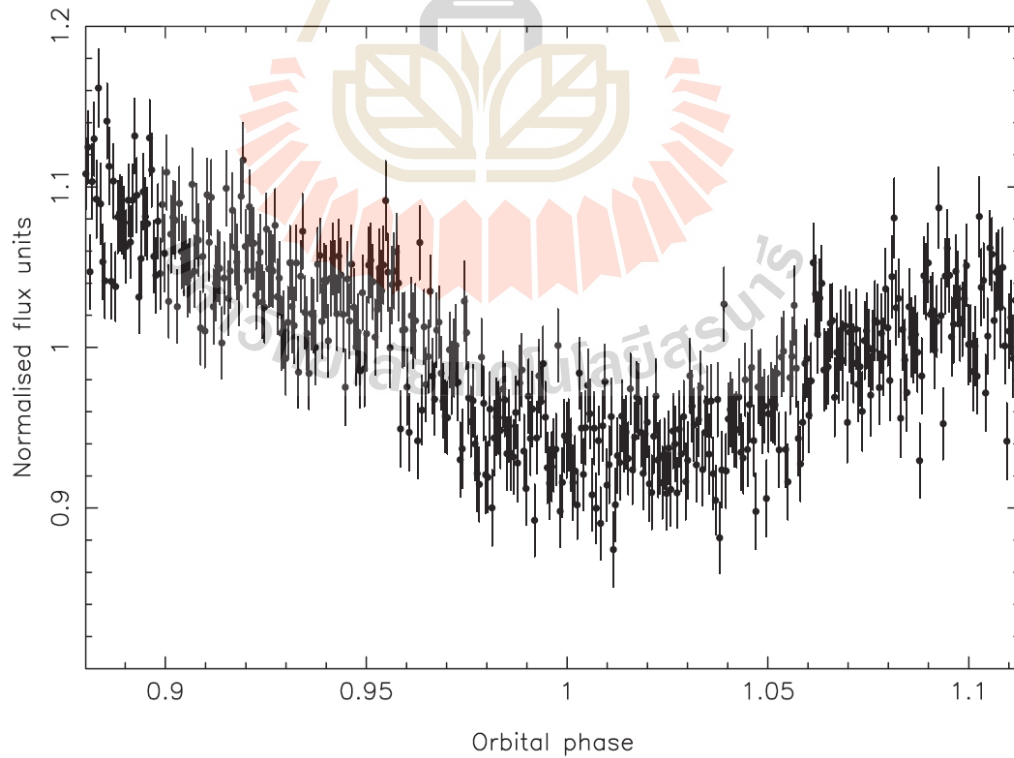


Figure 1.1 Light curve of SDSS J0745+2631 in r' filter from the follow-up observation (taken from Parsons et al., 2013).

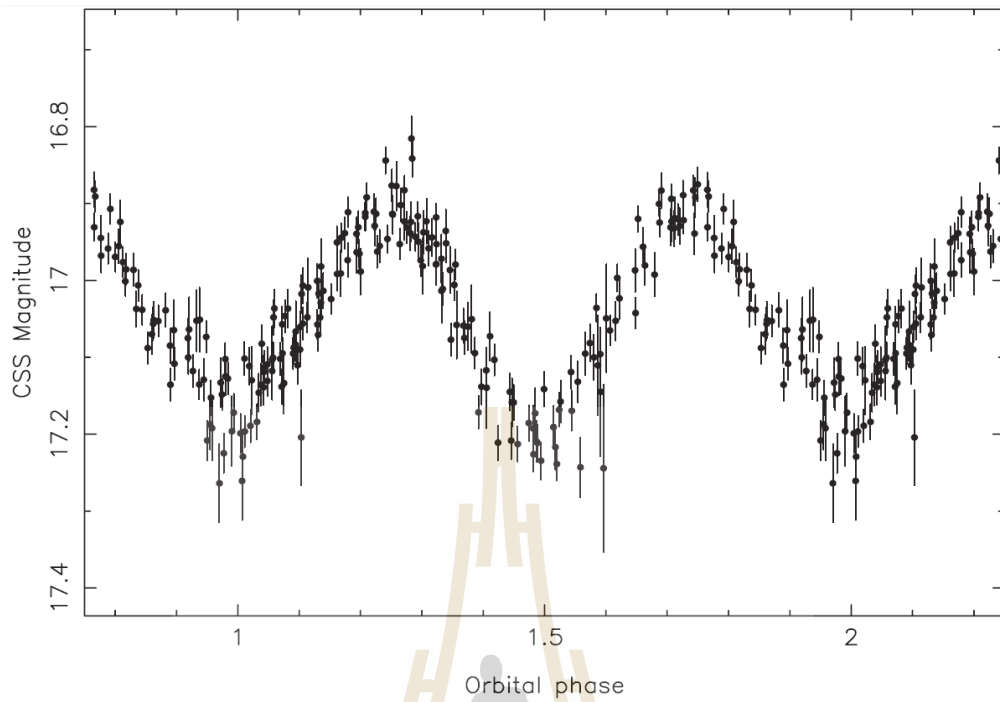


Figure 1.2 CSS light curve of SDSS J0745+2631 (taken from Parsons et al., 2013).

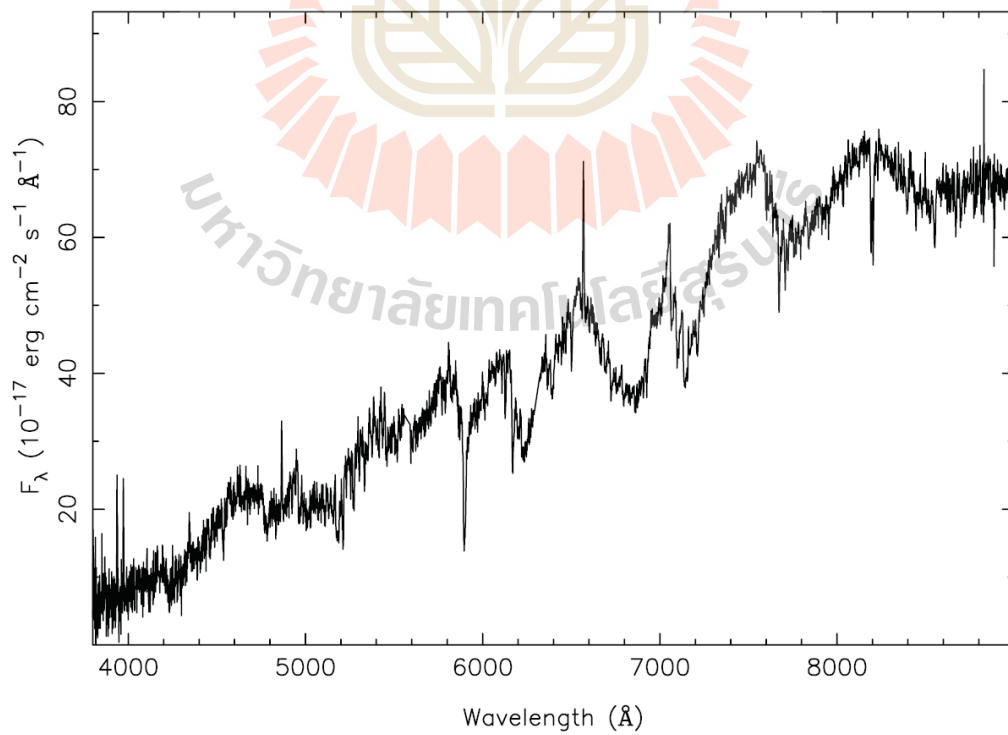


Figure 1.3 SDSS spectrum of SDSS J0745+2631 (taken from Parsons et al., 2013).

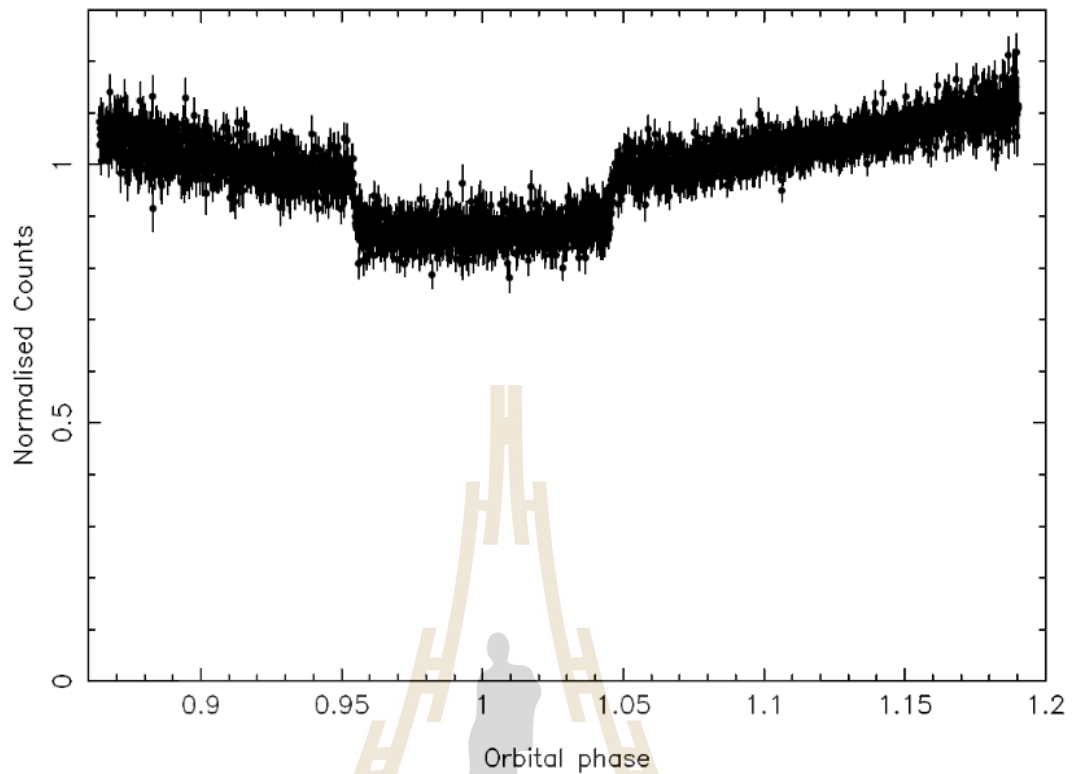


Figure 1.4 The light curve of SDSS J0745+2631 from High-speed ULTRACAM g' filter (taken from Parsons et al., 2015).

1.2 Research objectives

1. Obtaining light curves of SDSS J0745+2631.
2. Find mid-eclipse timing (T_0) and orbital period of SDSS J0745+2631.
3. Obtain physical parameters of SDSS J0745+2631 using BM 3.0 software and JKTEBOP code.

1.3 Scope and limitations of the study

SDSS J0745+2631 was observed using 2.4-meter TNT + ULTRASPEC in g' , r' and KG5 filters. The light curves was analyzed by using relative photometry method

with IRAF. The model of the orbital and stellar parameters will be derived using BM 3.0, and JKTEBOP code.



CHAPTER II

THEORY

2.1 Eclipsing binary

One of the fundamental studies about our nature is the study of celestial objects. This study mostly deals with the light coming from different objects in the sky, where the coming light were need to record and analyze for the understanding of the characteristic of the celestial objects. Eclipsing binaries are one type of variable stars which appear as a single point of light to an observer but these stars actually consist of two stars orbiting around their center of mass. Additionally, there are systems which host more than two stars and they are known as “multiple star system”. These type of systems contribute to ~20% of the binaries. The orbital period of the binary stars ranges from minutes to years, with visual binaries being the longest with a period that can reach up to tenth or hundreds of years.

Studying the feature of a light curve can tell us about the physical parameters and geometry of the binary components. Also, we can investigate the evolution of an eclipsing binary star by studying the crucial stages of the system when the stars undergo changes in their size. The feature of the light curve depends on many factors such as the Roche geometry of the stars, the mass ratio of the two components, the radius of each star, the orbital inclination of the system, and the effective temperature.

2.1.1 Two body system

When two stars of the binary system are close enough to each other, in which

their separation roughly equal to the diameter of the larger star, then the shape of the stars will be distorted due to the gravitational force and the stars will orbit under mutual gravitation attraction. While both stars of binary system orbit around their center of mass, the distance between them is compressed and expanded until the energy of the system is minimized and the momentum is constant. This state is often referred to as a “stable state” which will lead the system into synchronous rotation. The rotational period of the star is the same as the orbital period of the binary system in synchronous rotation.

To understand the effect of gravitational force in the close binary star system, the two body system of motion were considered.

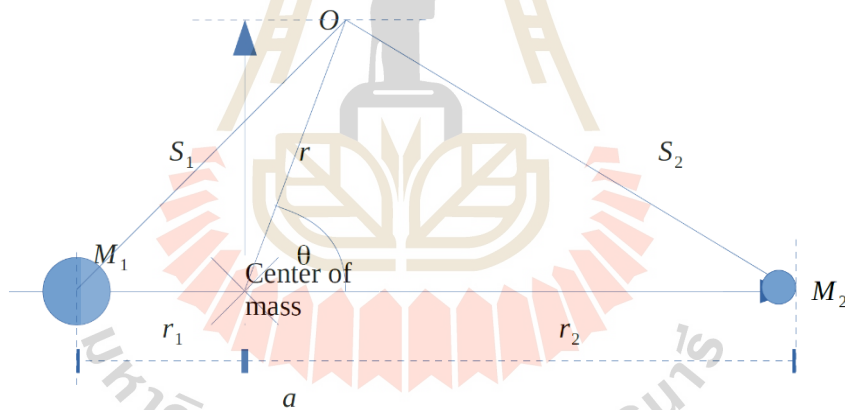


Figure 2.1 Jacobi coordinates for a binary star system.

Figure 2.1 shows a co-rotating coordinate for a binary system in which M_1 and M_2 represent the masses, and a represents the distance between M_1 and M_2 which also the sum of r_1 and r_2 . These stars are located on X-Y dimension at distances r_1 and r_2 , respectively, from the center of mass. Where O is the origin point and r is the distance from the origin to the center of mass. The orbital separation of two star is defined as a .

$$r_1 + r_2 = a \text{ and } M_1 r_1 = M_2 r_2 \quad (2.1)$$

2.1.2 The Roche Geometry

A binary system consists of a primary star with mass M_1 and a secondary star with mass M_2 ($M_1 > M_2$), at positions r_1 and r_2 from an arbitrary origin, under the assumption that the orbit is circular and the mass of each star is concentrated at its center, the total gravitational potential at the surfaces of the star is the sum of the potentials of the two stars and the centrifugal potential of the system as equation. The shapes of the equipotential come as a function of the mass ratio, $q = M_2/M_1$ as illustrated in Figure 2.2. If one of the star has expanded and fill the Roche lobe, mass transfer will take place through the inner Lagrange point L_1 , This point is very important for the close binary system. The transferred material will not fall to the other star directly but it will orbit around the companion in the form of a disk, also known as the accretion disk. The distance from L_1 to M_1 is denoted as

$$l_1 = a[0.500 - 0.227 \log(\frac{M_1}{M_2})] \quad (2.2)$$

and the distance from L_1 to M_2 is denoted as

$$l_2 = a[0.500 + 0.227 \log(\frac{M_2}{M_1})] \quad (2.3)$$

The shape of stars in binary star system is defined by the equipotential surface. The stars are spherical in shape when their radii are small relative to their separation ($R/a < 0.1$). When the star radius reach a limit where $R/a > 0.2$ then the star's shape become distorted from a spherical shape (Hilditch, 2001).

The important quantity for Roche lobe is the effective radius, or r_L the volume radius. Eggleton et al. (1983) derives an approximation of r_L with an accuracy of 1%.

$$r_L = \frac{0.49q^{2/3}}{0.69q^{2/3} + \ln(1+q^{1/3})} \quad (2.4)$$

The actual effective radius for the star at Roche lobe is $R_L = r_L a$, which a is the separation between two stars or semi-major axis and q is a mass ratio (M_2/M_1) of the stars.

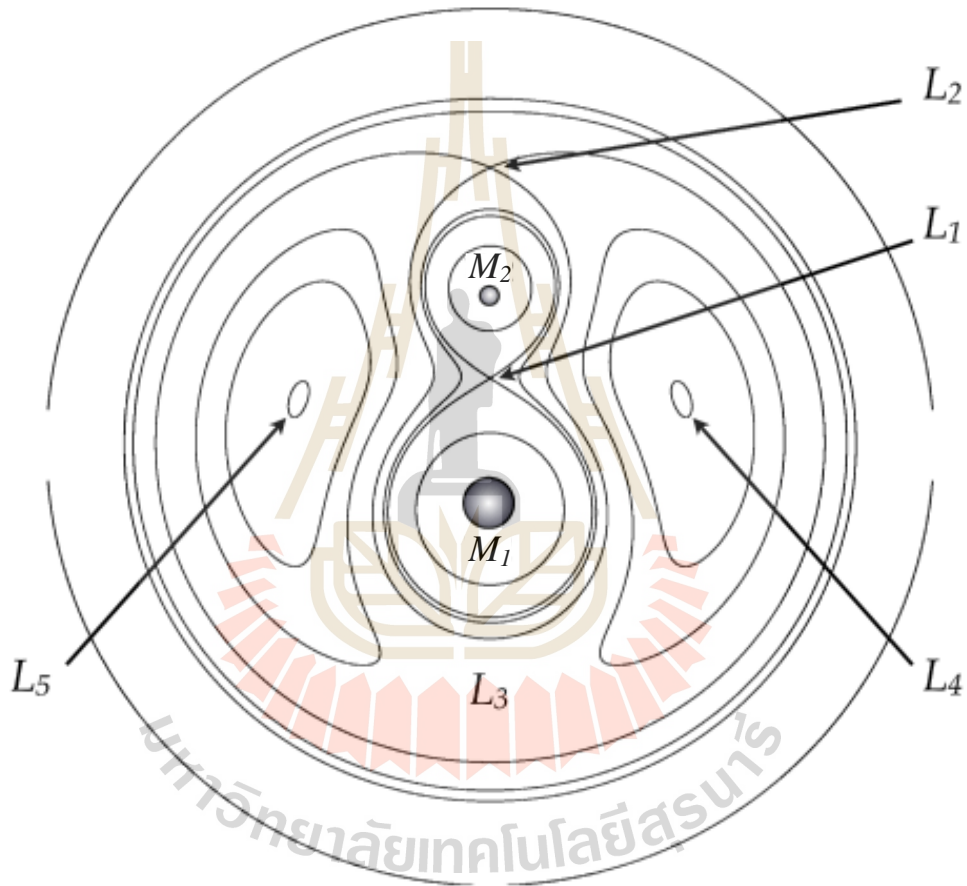


Figure 2.2 Cross section of equipotential surface of a binary system. The 5 points of gravitational potential in the binary star system are called the Lagrange points. The 3 points of gravitational potential (L_1 , L_2 and L_3) are located along the line that connects the two stars and the other 2 (L_4 and L_5) are located on the side. The inner Lagrange point (L_1) is called the Critical Roche lobe potential between 2 stars (Benacquista et al., 2013).

2.1.3 Limb darkening and reflection effect

Limb darkening is an effect seen in the stars, where the center of the star appears brighter than the edge. To understanding limb darkening, the idea of optical depth was considered, which means when the observer look at the edge of a star, the line of sight will be at an oblique angle to the stellar disk. The fact that the effective temperature of the stellar atmosphere is decreasing with an increasing distance from the center of the star. The limb darkening is given by an equation for the specific intensity

$$I(r) = I(0)[1 - u(1 - \sqrt{\frac{a^2 - r^2}{a^2}})] \quad (2.5)$$

where a is the radius of the star disk, r is the radius distance from the center of the disk and u is the *limb darkening coefficient*. This is can be written in the term of θ (see Figure 2.3) or $\mu = \cos\theta$:

$$I(r) = I(0)[1 - u(1 - \cos\theta)] = I(0)[1 - u(1 - \mu)] = I(0)(1 - u + u\cos\theta) \quad (2.6)$$

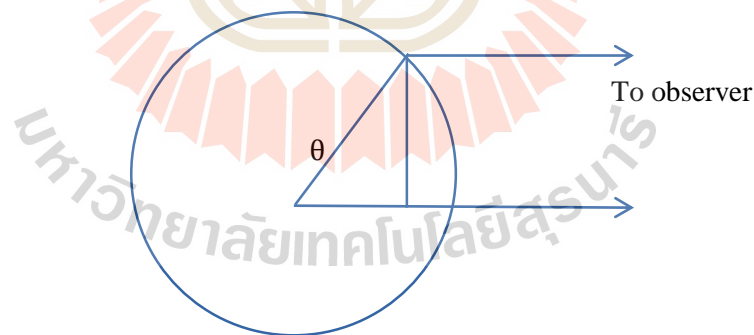


Figure 2.3 The cross section of star for the limb darkening effect.

The reflection effect is a phenomenon when flux from the radiative star strikes the surface of the other, its energy will heat up the receiving surface and generate more flux. The light curve can be explained in Figure 2.4, the surface of main-sequence star

is heated up due to the reflection effect of white dwarf especially around orbital phase 0.5.

2.1.4 Gravity darkening

Gravity darkening is an astronomical phenomenon when the star rotates rapidly, its shape will be an oblate spheroid. The radius at its equator is larger than its poles therefore the equator has lower surface gravity, lower temperature and brightness. Thus the equator is “gravity darkening”. However, gravity darkening also affects the tidally distorted stars in multiple systems. In 1924, Von Zeipel discovered that the surface flux is proportional to the value of the gravitational acceleration (g) and since the emergent flux and the effective temperature there exist the relation. The relationship between effective temperature and the gravitational acceleration is $T_{eff} \propto g_{eff}^{1/4}$.

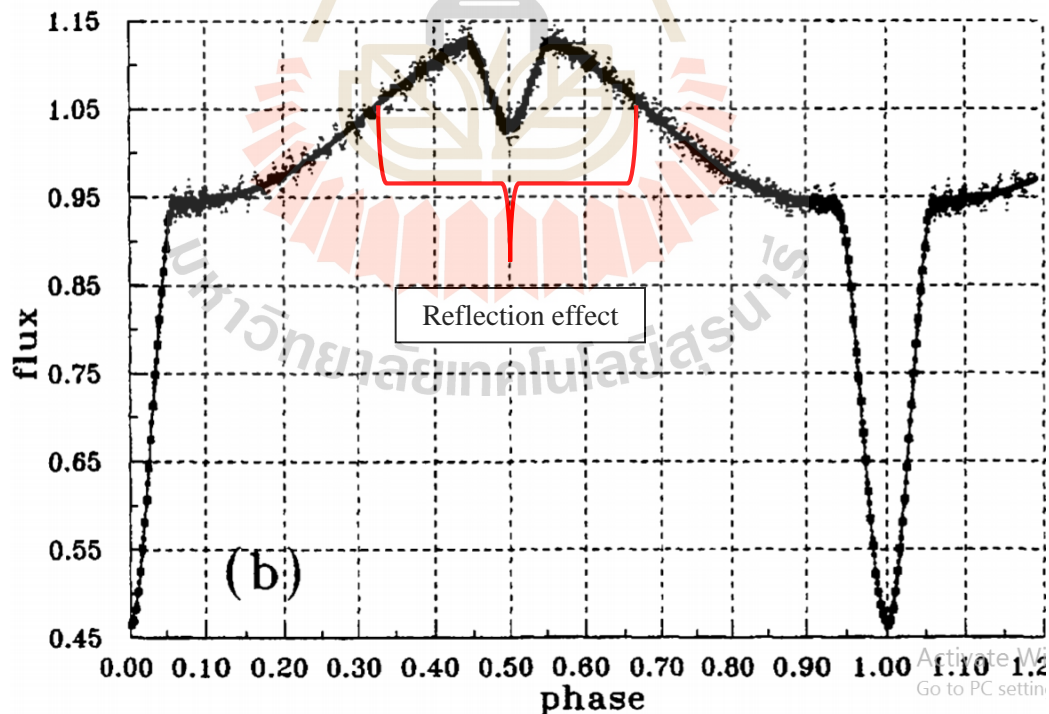


Figure 2.4 The light curve of PG 1336-018 shows a large effect of reflection (adopted from Sola et al., 1999).

2.1.5 Orbital parameters

The fundamental equation for light curve analysis can be derived using Newton's law of motion and Kepler's laws. From the observation and the light curve variation, assume the two members of the system are sphere, the eclipse can be used to determine the radii and the ratio of temperature. Consider the separation between two stars is not larger than the sum of the radii of them and assume that the inclination i (Figure 2.5) of the system is 90° (Carroll, 2014). Assuming that the light curve is produced with an inclination angle of almost 90° , the period and the radius of each star of the system can be considered as seen in Figure 2.5 and Figure 2.6.

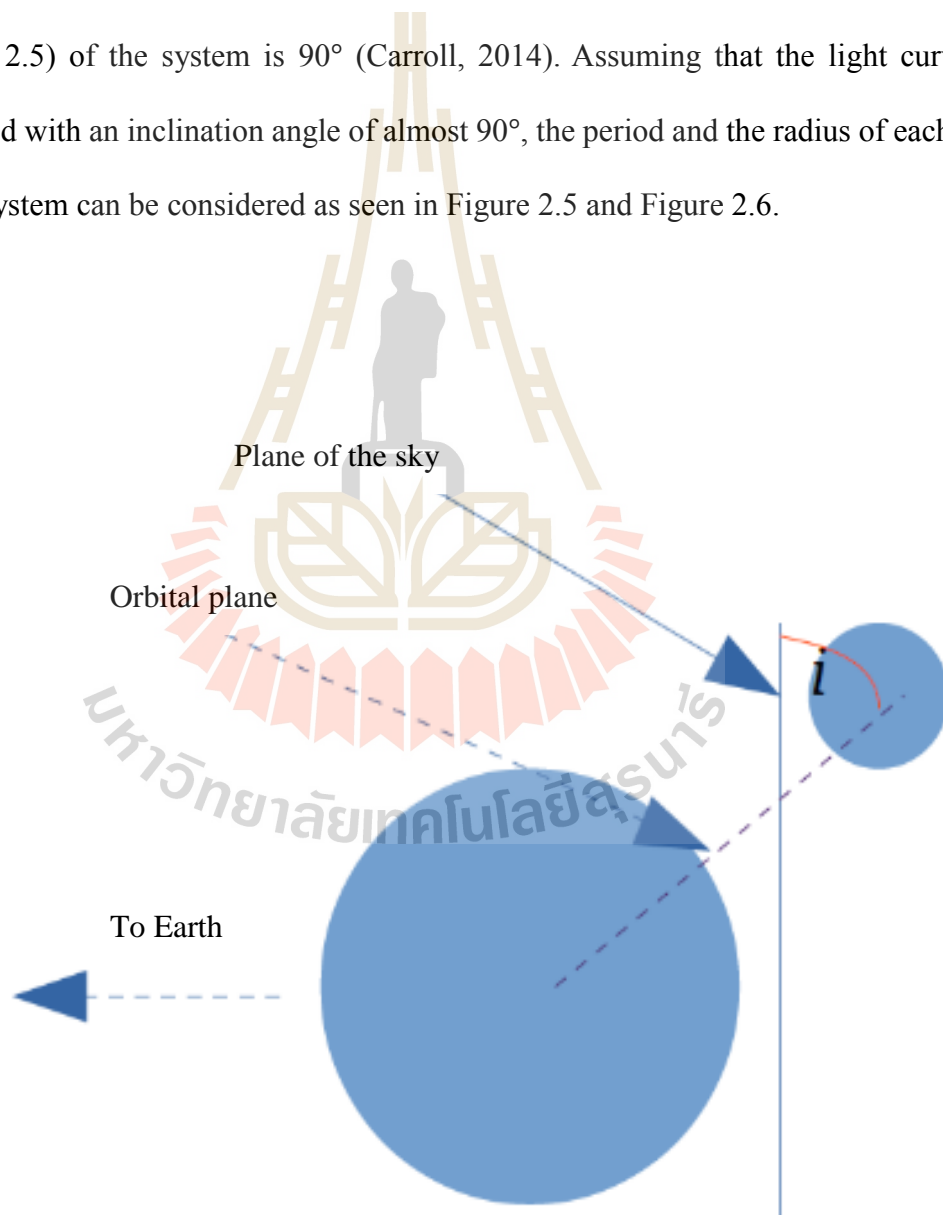


Figure 2.5 The geometry of an eclipsing binary with an inclination i .

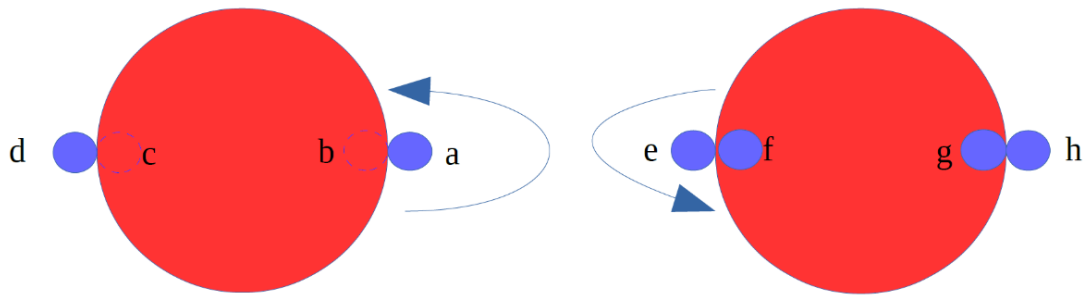


Figure 2.6 The binary star system, the smaller star is hotter than the larger one. The smaller star is orbit from the position a to d (the smaller star behind of the larger star) makes the primary eclipse. The smaller star is orbit from the position e to h (the smaller star in front of the larger star) makes the secondary eclipse.

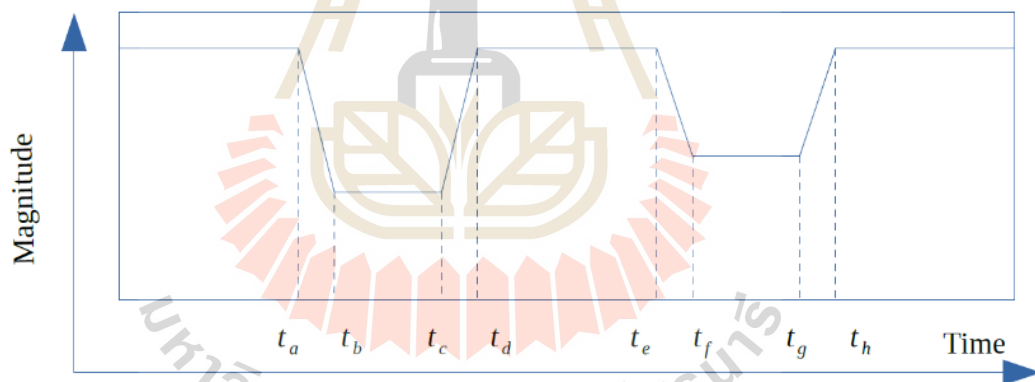


Figure 2.7 The light curve of an eclipsing binary with markers for the contact times.

The eclipse occurs when one of the star orbits pass another in the line of sight of the observer. Assuming that the brighter star (primary star) has smaller radius and the dimmer star has larger radius (secondary star) shown in Figure 2.7, the first contact time t_a is the time when the primary star is started to be blocked by the secondary star and this process is complete at time t_b . The time t_b to t_c is defined as the

primary eclipse timing, the time t_c is the time when the primary star is started to be unblocked by the secondary star and this process is completed at time t_d . Again, time t_e is the time when the secondary star is started to be blocked by the primary star and this process is completed at time t_f . The time from t_f to t_g is called the secondary eclipse timing. The time t_g is the time when the secondary star is started to be unblocked by the primary star and this process is completed at time t_h . Following the method described above, observation covering the full period of the binary will give us information on the radii of the primary (r_p) and the secondary star (r_s).

$$r_p = \frac{v}{2}(t_b - t_a) \quad (2.7)$$

Where the relative velocity of the two stars is v , $v = v_p + v_s$ in which v_p and v_s are the velocities of the primary star and the secondary star, respectively. Similar concept can be applied to find the radius of the larger star or secondary star (r_s).

$$r_s = \frac{v}{2}(t_c - t_a) = r_p + \frac{v}{2}(t_c - t_b) \quad (2.8)$$

From the light curve, the ratio of effective temperatures of the two stars derived by assuming the star as black body. The radiative surface flux F_r is given by the equation.

$$F_r = F_{surf} = \sigma T_{eff}^4 \quad (2.9)$$

Where F_{surf} is the flux at the surface of the star. T_{eff} is the effective temperature of the star. σ is the Boltmann constant $1.38064852 \times 10^{-23} \text{ m}^2\text{kg s}^{-2}\text{K}^{-1}$. When both stars are fully visible given by the total brightness B_o

$$B_o = k(\pi r_s^2 F_{rs} + \pi r_p^2 F_{rp}) \quad (2.10)$$

Where k is constant that depend on the distance from stars to the observer, F_{rs} is the radiative surface flux of the secondary star, F_{rp} is the radiative surface flux of the primary star. Then the amount of light from the primary star can be written as

$$B_p = k\pi r_s^2 F_{rs} \quad (2.11)$$

The other way round when the primary star (smaller, hotter star) is passing in front of secondary star, the flux is given by the equation below. For the secondary eclipse, the total brightness is

$$B_s = k(\pi r_s^2 - \pi r_p^2) F_{rs} + k\pi r_p^2 F_{rp} \quad (2.12)$$

The brightness ratio of the light curve is given as

$$\frac{B_o - B_p}{B_o - B_s} = \frac{F_{rp}}{F_{rs}} \quad (2.13)$$

And finally, the brightness ratio as

$$\frac{B_o - B_p}{B_o - B_s} = \left(\frac{T_{eff,p}}{T_{eff,s}} \right)^4 \quad (2.14)$$

2.1.6 Heliocentric correction

Julian Date (JD) is the amount of time that has passed, in days, since noon Universal Time (UT), the time in Greenwich, England, on January 1st, 4713 BC. However, if the binary system is in the plane of the Earth orbits about the Sun, the distance from Earth to a binary system can vary to 2 Astronomical Unit (AU) in 6 months, it corresponds to about 16 minutes of light traveling from the Sun to the Earth and also has an effect to time of the observation system as shown in Figure 2.8. Therefore, it is necessary to apply the corrections for the Earth's position of the plane. To correct the time, the Heliocentric Julian Days (HJD) was used where the Sun is the stable reference point of the observation. The Earth is an opposite site of the line of sight when viewed from the Sun. The HJD for every position of the Earth can be calculated using equation (2.15).

$$HJD = JD - \frac{r}{c} [\sin(\delta) \cdot \sin(\delta_{sun}) + \cos(\delta) \cdot \cos(\delta_{sun}) \cdot \cos(\alpha - \alpha_{sun})] \quad (2.15)$$

where r is the distance between Sun and observer, c is the speed of light α and δ are Right Ascension and Declination of our target and α_{sun} , δ_{sun} are Right Ascension and Declination of the Sun. As ULTRASPEC gives the time of observation in MJD , so for the correction of time MJD is converted to JD by equation (2.16).

$$JD = MJD + 2400000.5 \quad (2.16)$$

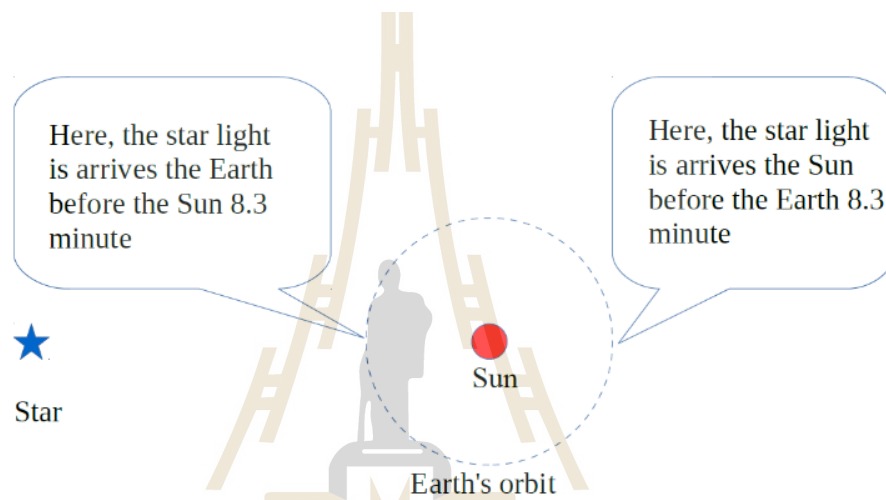


Figure 2.8 Light travel time as Earth revolves about the Sun.

2.1.7 Orbital period changes in eclipsing binary

As a result of the conservation of angular momentum when mass loss and angular momentum loss from the system, the orbital period of the system will also changes. From the analysis of the ephemeris curve, we can determine whether an eclipsing binary experiences a change in its orbital period by plotting between $O - C$ against the integer ϵ where $O - C$ is the time difference between the mid eclipse of the observation (O) and the mid-eclipse of the calculation (C) and ϵ is the number of eclipsing cycle. If we knew the previous of mid-eclipse time (T_0) then the next mid-eclipse could be calculated by using equation

$$C = T_0 + \epsilon P \quad (2.17)$$

where P is a period. The $O - C$ can be calculated using equation (2.18).

$$O - C = \Delta T(\epsilon) = O - T_0 - \epsilon P \quad (2.18)$$

The observed time of minimum, $O(\epsilon)$, is given by

$$O(\epsilon) = C(\epsilon) + \Delta(\epsilon) \quad (2.19)$$

where $C(\epsilon)$ is calculated from a linear ephemeris with an adopted period P_l

$$C(\epsilon) = T_0(\epsilon) + \epsilon P_l \quad (2.20)$$

The rate of change of the orbital period is calculated by equation

$$\frac{dP}{dt} = \dot{P} = \frac{dp}{d\epsilon} \frac{d\epsilon}{dt} = \frac{1}{P_l} \frac{dP}{d\epsilon} \quad (2.21)$$

2.2 Binary star evolution

The evolution of a binary system is depended upon the mass of its components in which the more massive will evolve faster than the less massive star. Binary star are categorized into three types from its Roche lobe radius. The Roche lobe is considered to be one of the important factor in binary evolution. If both stars are contained inside the Roche lobe, the system is known as detached binary system. If one of them has expanded over the size of its Roche lobe then it is a semi-detached binary. If both of them are have expanded and filled their Roche lobe then it is referred to as a contact binary system.

In most of its lifetime, a star stays in main-sequence phase where the hydrostatic equilibrium plays an important role. When the thermal pressure overcomes the gravitational force, the star will be expanded until fills its Roche lobe and it will transfer the material to the companion star through the inner Lagrange point (L_1). The processes

of mass transfer which are; (1) conservative mass transfer, all of the material from the donor star can accreted by the companion stars Figure 2.9, the donor star on the left side which transfers material to the companion star and create a accretion disk, this occurs before and after the first common envelope stage; (2) non-conservative mass transfer is the mass transfer but some of the mass is lost through $L_2 - L_3$; (3) stable mass transfer, the gainer can digest slowly the mass transferred by the primary. The gainer will slowly increase its mass; (4) unstable mass transfer, this is the one which will lead to CE phase, because the mass transfer happens so fast and the gainer cannot take the mass from the donor star, where the core of the donor and companion in the envelope of the donor star as seen in Figure 2.10. Most of the binary system may experience an unstable mass transfer phase in their evolution. The material is ejected from the envelope lead the system to the post common envelope stage.

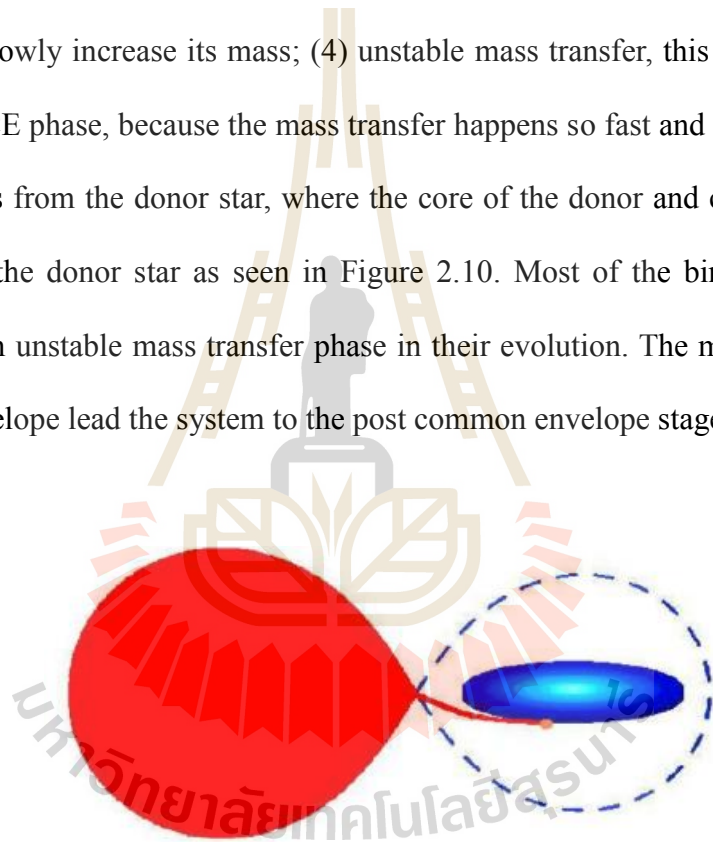


Figure 2.9 The conservative mass transfer after the first common envelope stage.

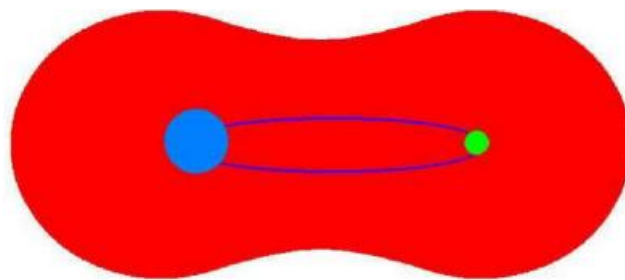


Figure 2.10 The common envelope stage.

2.2.1 Mass exchange

A star can reach the limit of its Roche lobe by expanding of the size through the normal stellar evolution process, the transition to giant or super giant star. There are three-time scales that are fundamentally important in the stellar structure and evolution, namely, the dynamical, thermal, and nuclear time scales. The dynamical time scale is the time required for a star to react to departure from hydrostatic equilibrium and it is defined as:

$$t_{dyn} = (2 R^3 / GM)^{1/2} \approx 40 \left[\left(\frac{R}{R_{\odot}} \right)^3 \frac{M_{\odot}}{M} \right]^{1/2} \text{ (minute)} \quad (2.22)$$

Where R is a radius of the star, R_{\odot} is a solar radius, M is a mass of the star, M_{\odot} is a solar mass, G is universal gravitational constant $G = 6.67408 \times 10^{-11} \text{ m}^3 \text{ kg}^{-1} \text{ s}^{-2}$.

The thermal time scale measures reaction time to depart from the thermal equilibrium where

$$t_{th} = \frac{GM^2}{RL} = (3.0 \times 10^7) \left(\frac{M}{M_{\odot}} \right)^2 \frac{L_{\odot}}{L} \frac{R_{\odot}}{R} \text{ (years)} \quad (2.23)$$

and the nuclear timescale is characteristic of the main-sequence lifetime, is

$$t_{nuc} = (7 \times 10^9) \frac{M}{M_{\odot}} \frac{L_{\odot}}{L} \text{ (years)} \quad (2.24)$$

Where L is the luminosity of the star. L_{\odot} is the luminosity of sun. The stellar radial on changes in mass, expand in the term $\zeta = (d \ln R) / (d \ln m)$. In 1987, Webbink described that the stellar radius changing in the mass of dynamical ζ_{dyn} , thermal ζ_{th} and nuclear ζ_{nuc} time scales can be compared with the stellar radius changing in the mass of the Roche lobe ζ_L as the mass ratio binary change. If $\zeta_L > \zeta_{dyn}$, the mass transfer will occur on a dynamical time scale because the star will not be able to adjust its hydrostatic equilibrium quickly enough to keep in pace with the Roche lobe change. If $\zeta_{dyn} >$

$\zeta_L > \zeta_{th}$, the mass transfer will take place on a much more gentle thermal time scale. If $\zeta_{dyn} > \zeta_{th} > \zeta_L$, then the star loses its mass only due to the stellar evolution processes (Hilditch, 2001).

2.2.1.1 Conservative mass transfer

The conservative mass transfer is a simple case that all the mass transferred by one component is gained by its companion. So $M_1 + M_2 = M_{tot}$, the lost mass of M_2 ($-dM_2$) is the accreted mass of M_1 (dM_1), $dM_1 = -dM_2$ and the total orbital angular momentum J_{orb} can be written as

$$J_{orb} = \left[\frac{GM_1^2 M_2^2 a(1-e^2)}{M_{tot}} \right]^{1/2} \quad (2.25)$$

and

$$\frac{\dot{P}}{P} = \frac{3\dot{M}_1(M_1 - M_2)}{M_1 M_2} \quad (2.26)$$

where M_1 is the masses of donor star, M_2 is the masses of an accretor star, P is the orbital period, these values after mass exchange, a is a semi major axis and e is an eccentric of the system, \dot{P} is differentiated orbital period with respect to time and \dot{m} is differentiated mass of star 1 with respect to time or the rate of mass flowing. If the initially more massive star transfers mass to the initial less massive star, then $\dot{M}_1 < 0$, the orbit shrink and $\dot{P} < 0$, the orbital period decrease. The period will keep decreasing until $M_1 = M_2$ and the orbital size has reached a minimum. If a star of mass M_1 continually losing mass after $M_1 < M_2$ then $\dot{P}_1 > 0$, and both P and a will increase again (Hilditch, 2001).

2.2.1.2 Non-conservative mass transfer

As an assumptions of conservative mass transfer, the total mass and angular momentum of the system is conserved, but they are not conserved for a non-

conservative mass transfer. The mass and angular momentum losing from the system. The simplest way of the mass and angular momentum losing from the system due to the stellar wind. In this case $\dot{J}_{orb} < 0$ and $\dot{M}_{tot} = -\dot{M}_1 < 0$, the orbital period and separation distance increase.

2.2.2 The formation of the common-envelope

The progenitor of the post common-envelope binary system typically composes of two main-sequence stars (as in Figure 2.11). The more massive star will evolve into the red giant branch faster than the less massive star. When the more massive star is evolved and filling its Roche lobe, the mass is transferred through the L_1 point. During the mass transfer process, the angular momentum is also transferred too. The separation between the stars and the size of the Roche lobe will decrease due to the conservation of the angular momentum in the system.

The binary orbit decays inside the common envelope because of friction and a loss of co-rotation between the core and envelope (Izzard et al., 2011). The secondary moves inside the envelope that can expels the envelope. The ejection process decreases the total mass and density of the common envelope (Izzard et al., 2011).

2.2.3 The common-envelope phase

The common-envelope is affected by hydrostatic and thermodynamic process of the star. In the evolution of the binary star, there is the ejection of envelope. Only some binary will undergo CE phase. Some CE will lead to merger, and some will lead to PCEB. The energy helps to expel or extract the envelope from the binary star is *common-envelope ejection efficiency* α_{ce} . This is defined as

$$\alpha_{ce} = \frac{\Delta E_{bind}}{\Delta E_{orb}} \quad (2.27)$$

Where ΔE_{bind} is the change in the binding energy of the *ejected* material and ΔE_{orb} is the change in the orbital energy of the binary star between the beginning and the end of the spiral process.

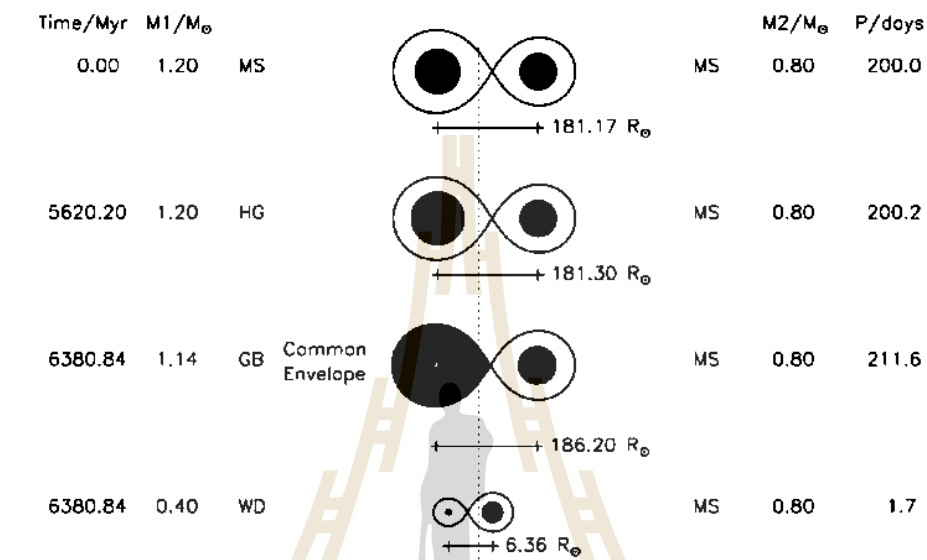


Figure 2.11 Schematic representation of the main evolutionary phases leading to the formation of a post-common-envelope binary. Where MS is represented main sequence star, HG is represented Hertzsprung gap, GB is represented giant branch, and WD is represented white dwarf. The more massive star is expanded size over the Roche lobe and then transfers mass to another. (taken from Willems et al., 2004).

2.2.4 Post-Common-Envelope

The binary star is covered with the envelope in the stage of the common envelope. In this stage, the envelope does not co-rotate with the binary and created the drag force which transfer the angular momentum and the energy from the binary system to CE as the orbital separation shrinkage. Eventually, the common-envelope is ejected and leave behind the binary system in the stage of post common-envelope. Normally,

the post common envelope has a short orbital period (<1 day) and consists of a white dwarf and main-sequence stars.

2.3 Physical properties of M-type star and White Dwarf

2.3.1 M-type star

In stellar evolution, the longest and stable phase in the lifetime of star is its main-sequence lifetime, where the star is in the thermal and hydrostatic equilibriums. The star has a nuclear fusion which converts hydrogen to helium and release the energy. However the main-sequence lifetime is depends on its total mass. The massive star have more gravitational potential energy, so they can collapse faster. As star collapse, the core of star has higher temperature, the result in faster nuclear reaction rates, the main-sequence lifetime is shorter. M-type stars are low mass main-sequence with characteristics as follow:

- The initial composition consists of about 70% of hydrogen, 28% of helium and trace amounts of other elements.
- The M-type star is undergoing fusion of hydrogen into helium within their cores.
- The core temperature has reached about 10 million K.
- The relationship between mass and luminosity is $L_{\odot} \sim 0.6M_{\odot}^{3.5}$.
- Low mass of M-type ($M < 1.5M_{\odot}$), the energy produced in the core is proton-proton (PP) chain, Energy source: hydrogen burning ($4\text{H} \rightarrow {}^4_1\text{He}$). For high mass of M-type ($M > 1.5M_{\odot}$), the core produces the energy in CNO cycle.

- The radiation dominates in the dense core and surrounding convective region.
- Lifetime: $T_{MS} \simeq 10^{10} \text{yr} \left(\frac{M}{M_{\odot}}\right)^{-3}$.

2.3.2 White Dwarf star

A white dwarf is represented to the last stage of stellar evolution. Through normal evolution channel, the white dwarf evolves from the main-sequence star into the red giant as in Figure 2.12. A carbon core formed at the center of the red giant, the core collapses into white dwarf and planetary nebula is ejected. Most of the white dwarf is made of Carbon and Oxygen. The mass of the white dwarfs in the Chandrasekhar limit, where the upper limit on the mass of a white dwarf approximately $1.39M_{\odot}$. The general properties of white dwarf as described by Fontaine et al. (2013) are:

- the temperature in range 3,000K to 200,000K.
- most of white dwarf have a mass close to $M \sim 0.6M_{\odot}$.
- the density in range $10^7 \text{ g}(\text{cm s}^{-2})$ to $10^9 \text{ g}(\text{cm s}^{-2})$.
- the gravitational acceleration is almost 400,000 times larger than at the Earth's surface.
- radius in range $0.006R_{\odot}$ to $0.025R_{\odot}$.
- the spectrum of white dwarf like a blackbody.

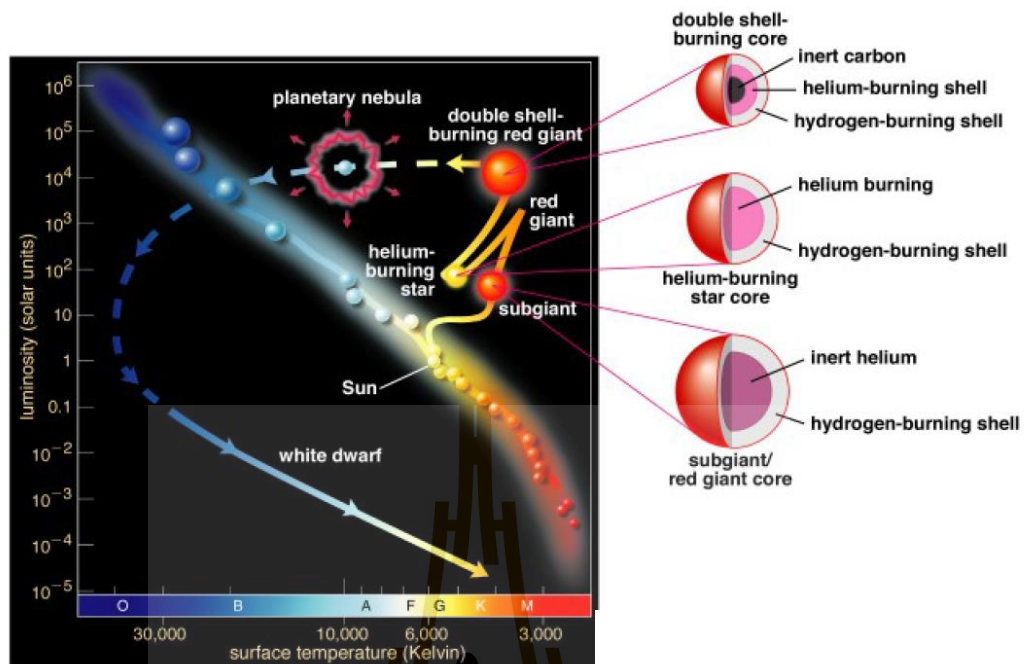


Figure 2.12 The evolution of a normal star. The main-sequence star evolved to the red giant or super giant with hydrogen burning by nuclear fusion, the heavier elements are inside the core. Helium core burns into carbon and oxygen and eventually helium shell burning with a carbon core formed at the center of the star planetary nebula is ejected (25 - 60% of mass ejected) expands for about 50,000 years before fading core collapses into white dwarf at center of planetary nebula (adopted from Bradley et al., 2014).

CHAPTER III

METHODOLOGY

Most of the astronomy study deal with a point source of signal from space using the telescope and other instruments. In this chapter, the methods and techniques are presented for correction and to analyze the data.

3.1 Observation

3.1.1 Target selection

In this study, we focus on an eclipsing binary system with one component is a white dwarf star (WD) and the other one is a main-sequence star (MS). In 2013 Parsons and his colleagues published the newly eclipsing PCEBs from Sloan Digital Sky Survey (SDSS) and Catalina Sky Survey (CSS). Among those, SDSS J0745+2631 is recognized as a WDMS due to the blue excess in its spectra. SDSS J0745+2631 is an interesting object to study because Parsons et al. (2013) classified this binary as a possible eclipsing system, although they could not confirm the eclipses from their photometric data. A more recent paper by the same author (Parsons et al., 2015) gave confirmation on the eclipses in J0745+2631, but there is no report of orbital parameters of this system.

STARALT program was used for the visibility chart of SDSS J0745+2631 in each observation night. An example of object visibility of SDSS J0745+2631 is shown in Figure 3.1.

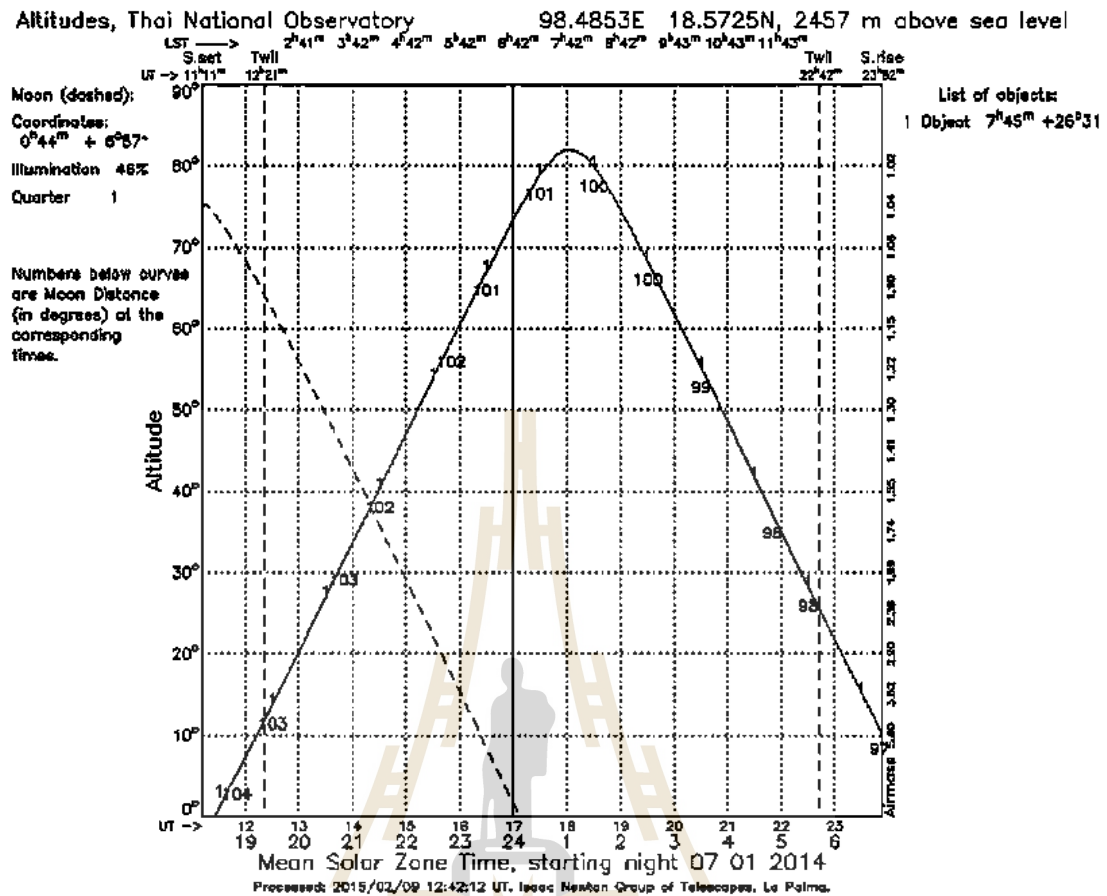


Figure 3.1 The visibility chart of SDSS J0745+2631 on the night of 7th January 2014.

The dashed line is moon's position and the solid line is the target's position throughout the night. The y1-axis is the altitude of the celestial object. While y2-axis gives the air mass values. The x-axis is times, the upper one is time in UT and the lower one is the local time of the observational site.

STARALT (available on the website of the Isaac Newton Telescope group, <http://catserver.ing.iac.es/staralt/>) is a program that shows the observability of celestial objects which plot the altitude against time for a particular night. This program gives the information of the phase, the rising time, and the setting time of the Moon and the target for a certain location. It also calculates the distance of the target to the Moon.

3.1.2 Telescope: Thai National Telescope (TNT)

The Thai National Observatory (TNO) houses the Thai National Telescope (TNT), a telescope with a 2.4-meter primary mirror, and a Ritchey-Chretien optical layout with an $f/10$ focal ratio, providing a plate scale of $8.6''/\text{mm}$ at the two Nasmyth foci. TNO is located at Doi Inthanon, Thailand (shown in Figure 3.2).



Figure 3.2 Left: Thai National Telescope 2.4-meter. The mirror covers are open and the 2.4-meter primary. Right: the Thai National Observatory, the 2.4-meter TNT in the dome which besides control building (retrieved from <http://www.narit.or.th/>).

The TNT was designed and built by EOS Technologies. The telescope is only operated in the dry season, from November to the April. The instrument provides a good observational data in the clear night sky. It can observe a star with a magnitude as faint as $B=22.5$ and $V=21.9$ magnitude arcsec^{-2} . All of data are taken using the ULTRASPEC instrument installed at the 2.4-meter telescope. Using ULTRASPEC offers the low readout noise and excellent readout time which is suitable for fast photometry. ULTRASPEC can work across the optical wavelength range of 330 - 1000 nm, which is covered by the Sloan filter system (Dhillon et al., 2014).

3.1.3 ULTRASPEC

ULTRASPEC is a high-speed, frame-transfer camera based on electron multiplying CCDs (EMCCDs) with the image area 1024×1024 pixels and the data acquisition system of ULTRACAM (Dhillon et al., 2014). The detector is an E2V CCD 201-20 where the dead time is almost negligible which close to zero readout noise when a frame is transferred with high-speed frame rates. The readout noise is 2.3 e^- with normal output. The frame-transfer EMCCD chip mounted in the cryostat is shown in Figure 3.3. The ULTRASPEC CCD is cooled down below 160 K by liquid nitrogen, where the thermal noise of about $10 \text{ e}^-/\text{pixel}\cdot\text{h}$ and the dark current is almost negligible. High-speed photometry enables the study of compact objects, such as white dwarfs, neutron stars and black holes because ULTRASPEC is capable of detecting seconds and sub-seconds variability from an object (Dhillon et al., 2014).

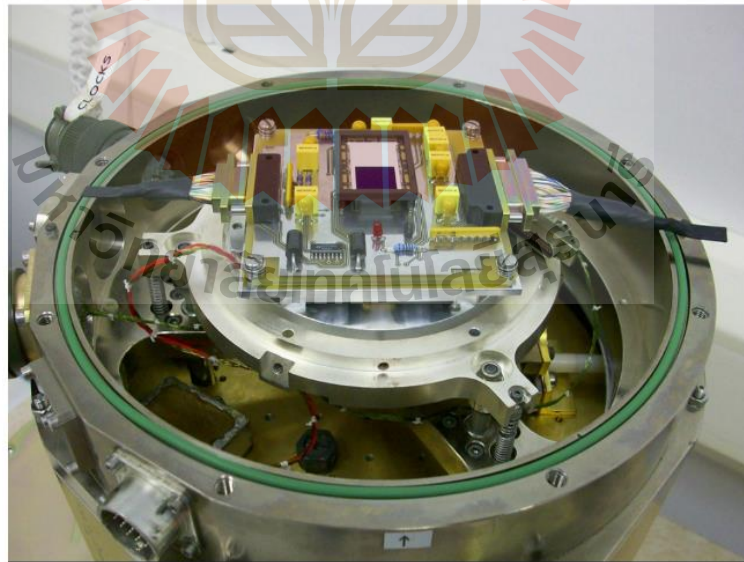


Figure 3.3 The frame-transfer EMCCD chip mounted in the cryostat. (credit : V.Dhillon (photographer); retrieved from <https://www.flickr.com/photos/68020802@N03/sets/72157633629346788/>).

The ULTRASPEC is designed to overcome the problem of slow read out by using the principle of electron-multiplying and frame-transfer as seen in Figure 3.4. The ULTRASPEC works with 3 clocks of the storage area. One is the vertical clocking for collection the signal in the vertical line and the other two clocks are the horizontal clocking for normal and avalanche output. The high-voltage is used for inducing electron and transferring photoelectrons in the electron-multiplication register. It also generates new electron via impact ionization. The avalanche multiplication creates new electron in a process similar to a chain reaction (Ives et al., 2008).

3.1.4 Data acquisition system

The data acquisition system for TNT+ULTRASPEC is the ULTRACAM pipeline. The data acquisition hardware used in the ULTRASPEC is shown in Figure 3.5 (visit: <http://deneb.astro.warwick.ac.uk/phsaap/software/ultracam/html/index.html>, for more information).

The data was taken by the ULTRASPEC and then are being read out by a San Diego State University (SDSU) controller. The SDSU controller is hosted by a rack-mounted, quad-core PC running Linux patched with Real Time Application Interface (RTAI) extensions (Dhillon et al., 2014).

3.1.5 Filters

Stars radiate energy in different wavelengths depending on their temperatures and characteristics, so it is necessary to choose the appropriate filters for the observation. The SDSS filters are used to take the data of J0745+2631. These filters are mounted on the filter wheel as seen in Figure 3.6 and the transmission profiles of the SDSS filter in Figure 3.7. The detailed information of the SDSS filters are presented in Table 3.1.

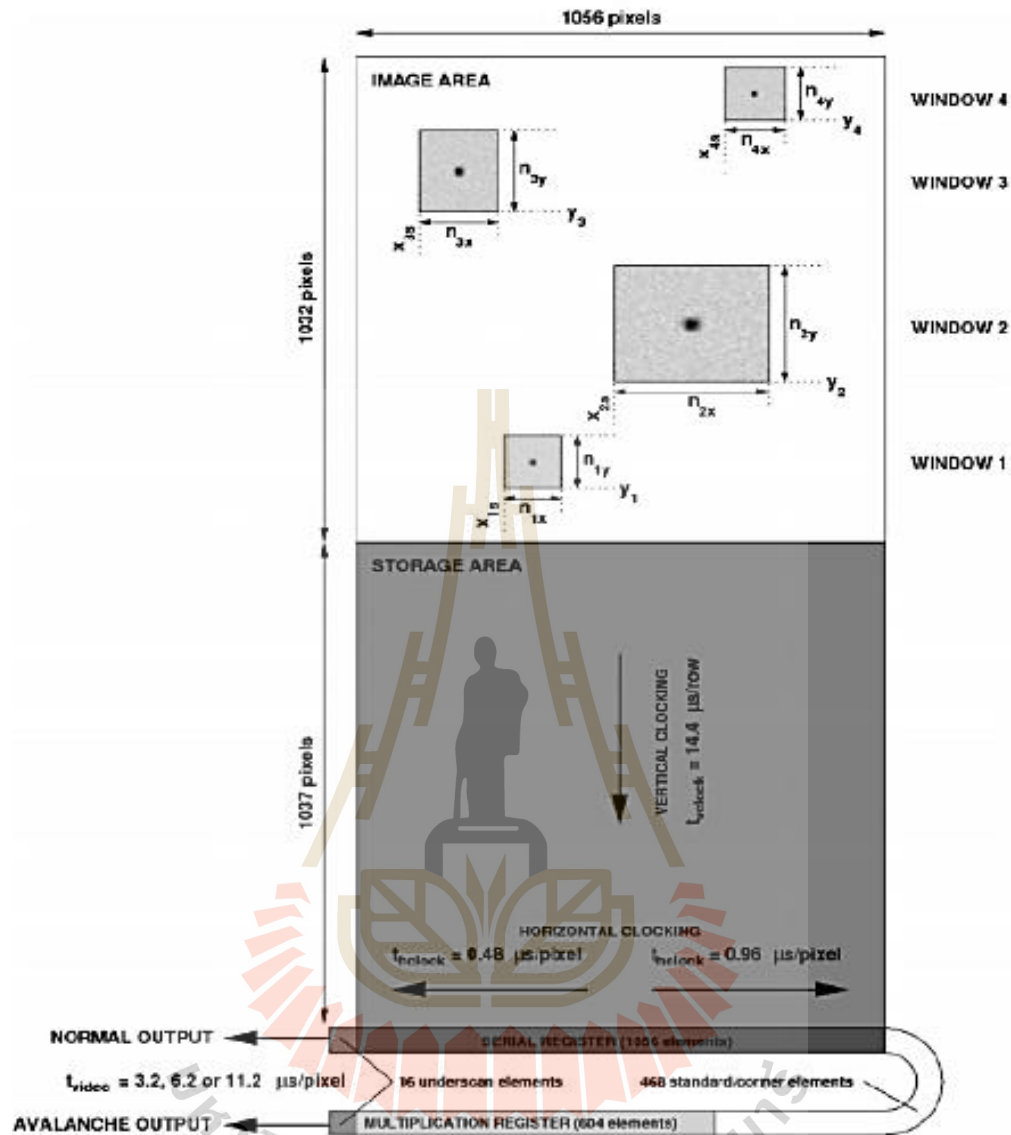


Figure 3.4 The diagram of the ULTRASPEC EMCCD. There are two main areas, the image area and the storage area. For the fast readout, the image area can offer up to 4 sub-windows to the observer. The electron transfers from the image area to the storage area. The 3 clocks were used for the time correcting, one of vertical clock and two of horizontal clocks for collecting electron and each electron will be duplicated in the processes of electron-multiplication or impact ionization, the result of the impact ionization gives 1000 electrons per 1 incident electron (taken from Dhillon et al., 2014).

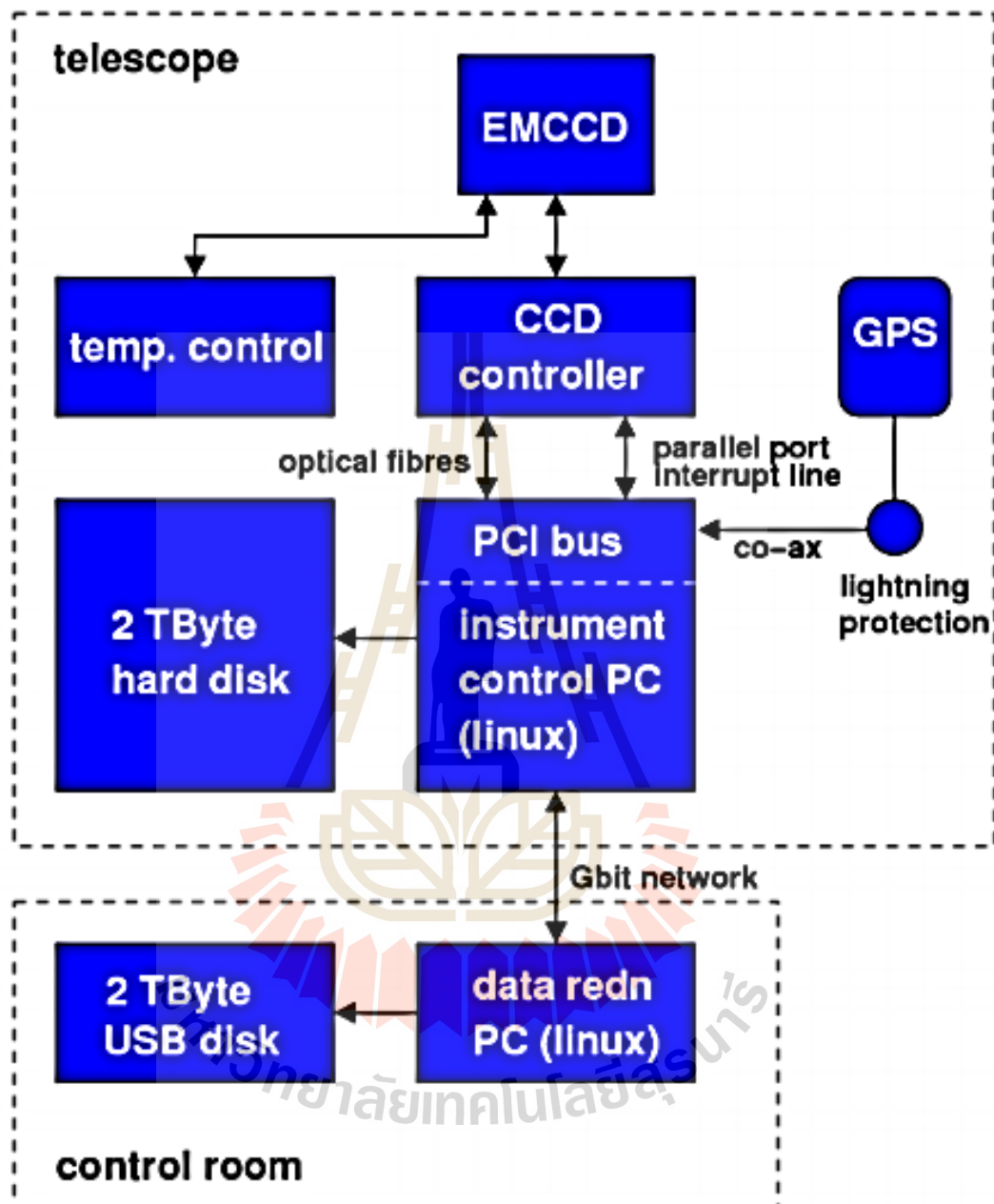


Figure 3.5 The diagram showing the principal hardware components of ULTRASPEC data acquisition system (taken from Dhillon et al., 2014).

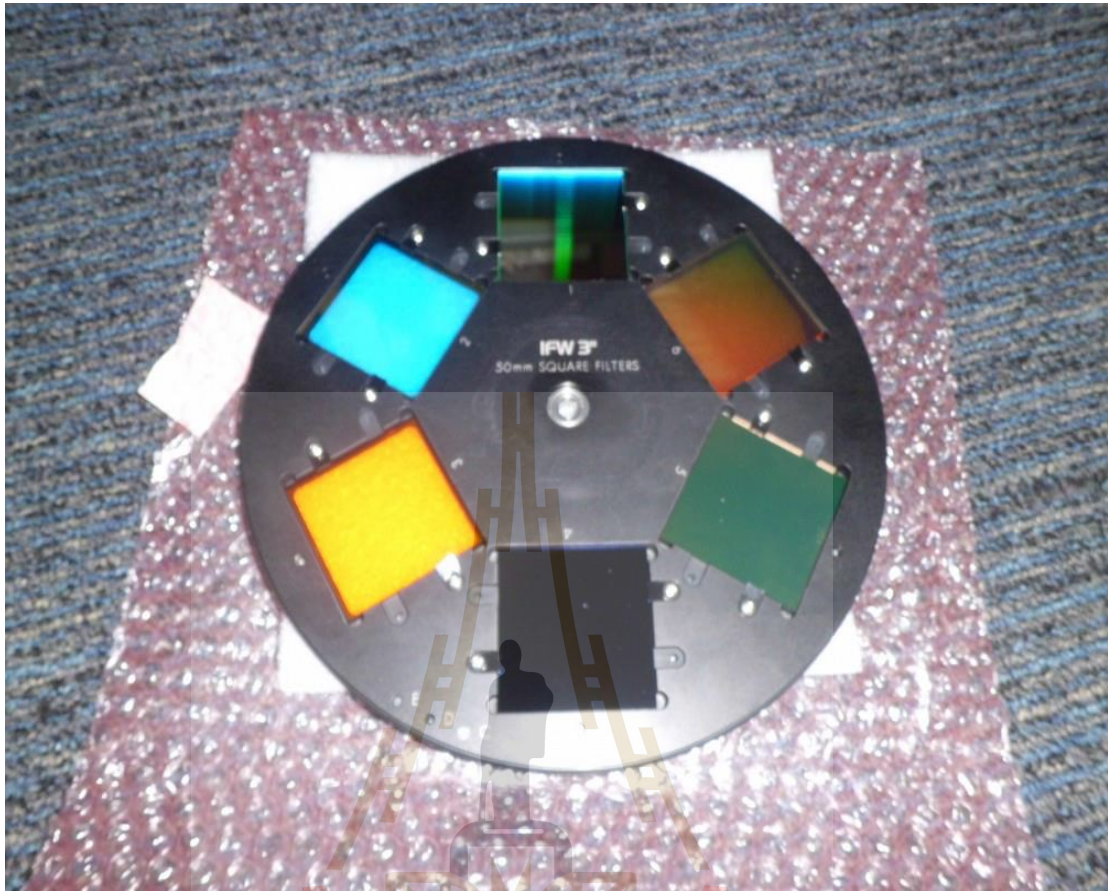


Figure 3.6 The filter wheel of the ULTRASPEC, showing six slots with the filters mount on each slot. (credit: V.Dhillon (photographer); retrieved from <https://www.flickr.com/photos/68020802@N03/albums/72157635036605871>).

3.1.6 Observation data

Our first observation was performed on 7th January 2014 at the Thai National Observatory (TNO). The other observations were taken in the end of 2014, on 20th and 22nd December 2014, and the last observation was done in 2016, during 8th-11th January 2016. A complete log of the observations is given in Table 3.2.

Figure 3.7 shows the transmission profiles of the ULTRASPEC SDSS filter.

The dotted line represents the anti-reflection coatings used on the ULTRASPEC lenses. The dashed-dotted line is the transmission of the atmosphere for unit air mass. The dashed line is the quantum efficiency curve of the ULTRASPEC EMCCD.

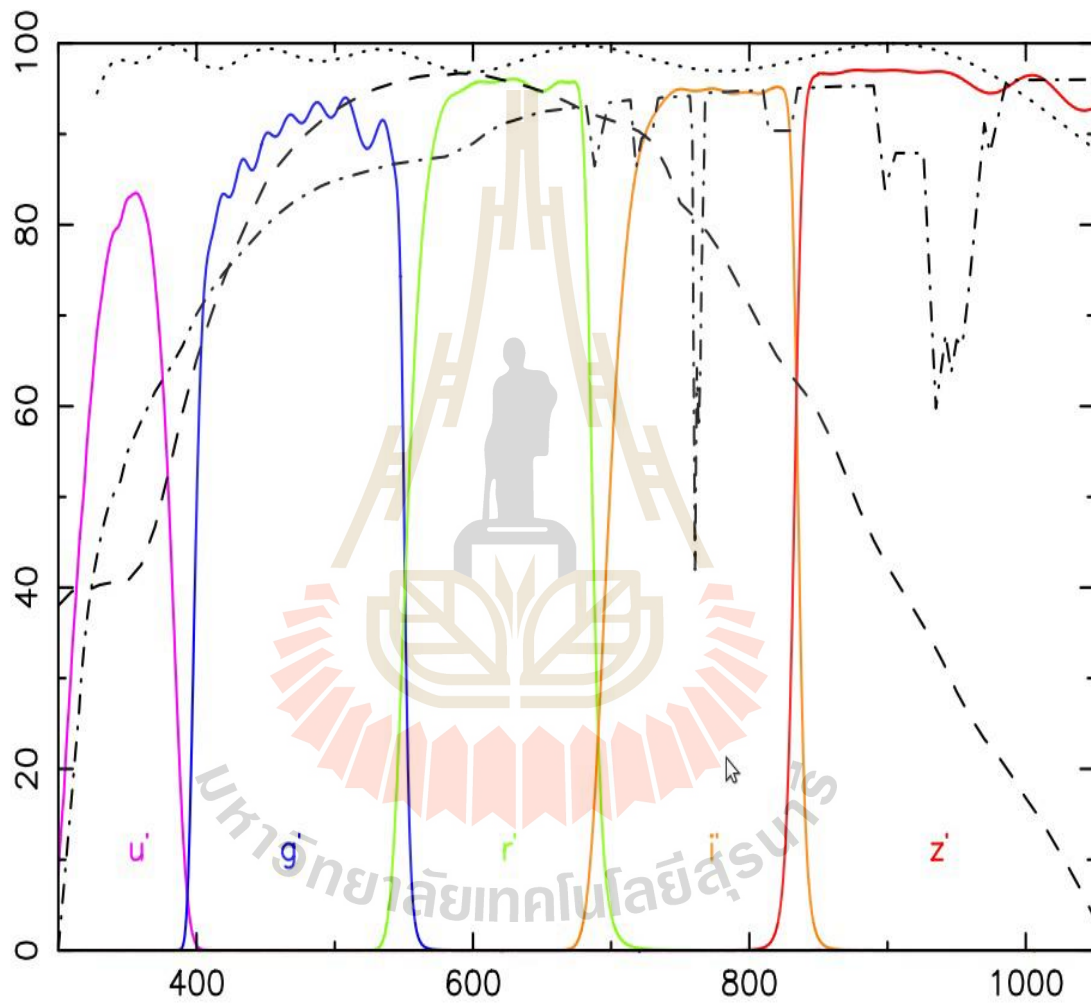


Figure 3.7 The transmission profiles of the ULTRASPEC SDSS filter set (purple, blue, green, orange and red solid lines correspond to u' , g' , r' , i' and z' , respectively) (taken from Dhillon et al., 2014).

Table 3.1 ULTRASPEC filters. λ_c is the central wavelength and $\Delta\lambda$, $\Delta\lambda_c$ are the FWHM.

| Filter | $\lambda_c(\text{nm})$ | $\Delta\lambda(\text{nm})$ |
|----------------|------------------------|----------------------------|
| u' | 355.7 | 59.9 |
| g' | 482.5 | 137.9 |
| r' | 626.1 | 138.2 |
| i' | 767.2 | 153.5 |
| z' | 909.7 | 137.0 |
| Clear | - | - |
| Schoot KG5 | 507.5 | 360.5 |
| $i'+z'$ | 838.5 | 290.5 |
| CIII/NIII+HeII | 465.7 | 11.2 |
| Blue continuum | 514.9 | 15.8 |
| NaI | 591.1 | 31.2 |
| Red continuum | 601.0 | 11.8 |

3.2 Data reduction

In any astronomical observation cannot avoid noise completely. Usually, noise is divided into four main types. The first is an intrinsic noise: it originates in the detector. This type of noise depends on the characteristic of the detector. The second type of noise is a signal noise: this type is arising from the characteristic of the incoming signal,

especially the quantum nature. The third type of noise is an external noise: this type of noise is coming with an unwanted signal such as cosmic ray etc. The fourth type of noise is a processing noise: this noise arising from amplifiers used in converting the signal from the detector. So, we need to remove noise from the image as much as possible for the best result.

Table 3.2 Photometric observations of SDSS J0745 +2631. The primary eclipse occurs at phase 1, 2 etc.

| Date | filter | Time of observation (UT) | Exposure time (second) | phase | Conditions (Transparency, seeing) |
|-------------|--------|--------------------------------|------------------------------|-------------|---|
| 7 Jan 2014 | g' | 16:30 – 20:00 | 8 | 0.467-1.130 | 2.0-4.0 |
| 20 Dec 2014 | r' | 18:08 – 23:03 | 9 | 0.342-1.279 | 2.5-5.0 |
| 22 Dec 2014 | KG5 | 14:30 – 17:04 | 8 | 0.754-1.242 | 3.0-5.0 |
| | g' | 20:32 – 21:37 | 3 | 0.921-1.126 | 3.0-5.0 |
| 8 Jan 2016 | g' | 14:25 - 20:26 | 5 | 0.950-2.093 | 3.0-6.0 |
| 9 Jan 2016 | KG5 | 21:39 - 22:30 | 3 | 0.886-1.048 | 3.0-6.0 |
| 10 Jan 2016 | KG5 | 13:28 - 15:39 | 7 | 0.893-1.306 | 3.0-6.0 |
| 11 Jan 2016 | g' | 15:16 – 17:03 | 6 | 0.787-1.128 | 3.0-5.0 |

The calibration is the process of subtracting the bias and dark signal and then divided by flat signal. The equation below represent the procedure for calibrating a raw

science image into a clean, processed science image.

$$\text{Calibrated image} = \frac{(\text{Raw image}) - (\text{Master Bias})}{\text{Master Flat}} \quad (3.1)$$

Where *Master Bias* is an offset that occurs when a pixel is read from the CCD camera and *Master Flat* is an exposed image with the entire field of view of the image as uniformly as possible.

When we observe the astronomical object, it means that we are dealing with many correction images in each type bias and flat. But in the processing of calibration we only need one of them and we call them *Master Flat* and *Master Bias*. The *Calibrated images* is the result of the *Bias images* subtraction from *Raw images* and *Master Flat* images division as in equation (3.1) and the process of the calibration is shown in Figure 3.8.

After the calibration process, the science images or clean image and ready to do photometry. In this thesis, IRAF was used for image reduction and photometry process. IRAF is the acronym for Image Reduction and Analysis Facility, a general purpose software system for the reduction and analysis of astronomical data.

3.2.1 Bias-subtraction

A bias frame is referred to the image frame recording count with zero exposure time. Bias frame is the background counts of the instrument. The bias count needs to be removed from all of type data frames. In practice many bias frames were taken so the count subtraction of bias frame from a celestial images need to combine several *Bias images* to get the average level of bias count which is called *Master Bias image*.

3.2.2 Flat-fielding

The reason for flat-fielding is to avoid the defect in the image. Most CCDs are nearly perfect when they were first made, but over the year the CCD is accumulating many contaminants such as oil, grease and dust etc. There are also some dust on a CCD and the telescope mirror which are blocking light from source and makes the doughnut pattern image. The pattern is an unwanted result. So in a *Calibration images*, this effect need to be removed by dividing the *Raw images* with the count of *Flat images*.

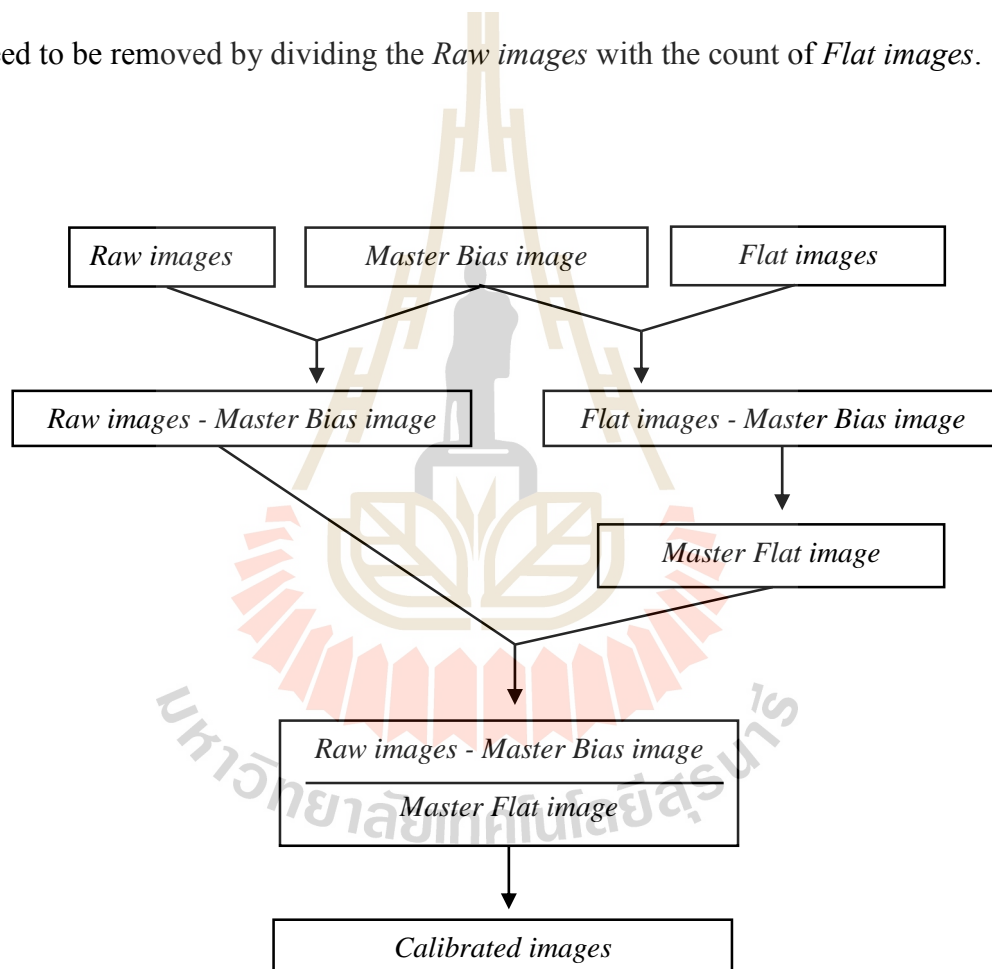


Figure 3.8 Flow chart of the data reduction processing.

3.2.3 The photometry with IRAF

After bias and flat corrections, the *clean image* is ready for photometry. But

sometimes the position of the star shifts in each image. Although the telescope can track the target precisely but there is some event happen during observation such as the limit of the telescope when the target star transit, this make the telescope stop its tracking rotate and slew. So, the position of each star in all of the images need the same. These problems are overcome by using *imalign* task in *imarith* package of IRAF. To measure the flux from the star, the aperture radius is defined by a *moffat function* of the star profile. The sky background is calculated and subtracted from the target star, using a predefined annulus. The photometric data reduction gives the output such as count, magnitude and error magnitude of the star. The analyzed data provide a light curve in which the target's flux is divided by the comparison's flux or the target's magnitude minus by comparison's magnitude. The variation of the light curves due to atmosphere can be removed using this method.

3.3 Data analysis

3.3.1 Calculation of correction to the observation time

For more correction of observation, the time is changed from Modified Julian Date (*MJD*) to Julian Date (*JD*) and *JD* is changed to Heliocentric Julian Date (*HJD*). The conversion of each *MJD* to *JD* uses the relation of equation (2.16). Then *JD* is changed to *HJD* uses equation (2.15). If the binary system is in ecliptic plane, changing *MJD* to *HJD* given us more precise time which *MJD* and *HJD* can be different 16 minutes.

3.3.2 Calculation of the relative flux

The light curve is analyzed by using the relative flux method which the y axis is the relative flux of target/reference star and the x axis is the time or the orbital phase.

The reference star should have constant brightness (non-variable star). Also, the reference star was checked with other non-variable star to confirm that the reference star is not varying in brightness and all of them should be in the same field of view.

3.3.3 Calculation of orbital phase

A binary star system's ephemeris is used for converting the *HJD* from the observation into orbital period value. The ephemeris is a formula for calculating the times of minimum light (or times of primary eclipses). The Figure 3.9 shows light curve from observing night of 7th January 2014 with *HJD* as x axis and relative flux as y axis. The middle of the Figure 3.9 shows light curve 7th January 2014 night with orbital phase as x axis and relative flux as y axis. The top and bottom of Figure 3.9 show light curves of observing night 7th January 2014 with using 2 differences of time in the calculation of orbital phase. The eclipse duration is about 28 minute and in orbital phase of 0.95-1.05.

3.4 Light curve modeling

The two programs were used for modeling eclipsing binary star system, first one is the BM 3.0 and the second program is JKTEBOP.

3.4.1 Binary Maker 3.0

BM 3.0 is a program for modeling light curve of the eclipsing binary star (Bradstreet and Steelman, 2004). The BM 3.0 needs a normalized light curve with the x-axis is represented by orbital phase and the y-axis is represented by the relative flux. For the usage of BM 3.0, we need to put the initial parameters of the system to the program such as the effective temperature of each star, wavelength, radii, mass ratio, the reflection effect of the star, limb darkening. The expected result of the program

should give us the proper synthetic light curve. Also, BM 3.0 give us the 3D model of the orbiting stars. This is very useful for the understanding of the feature of the eclipsing binary star.

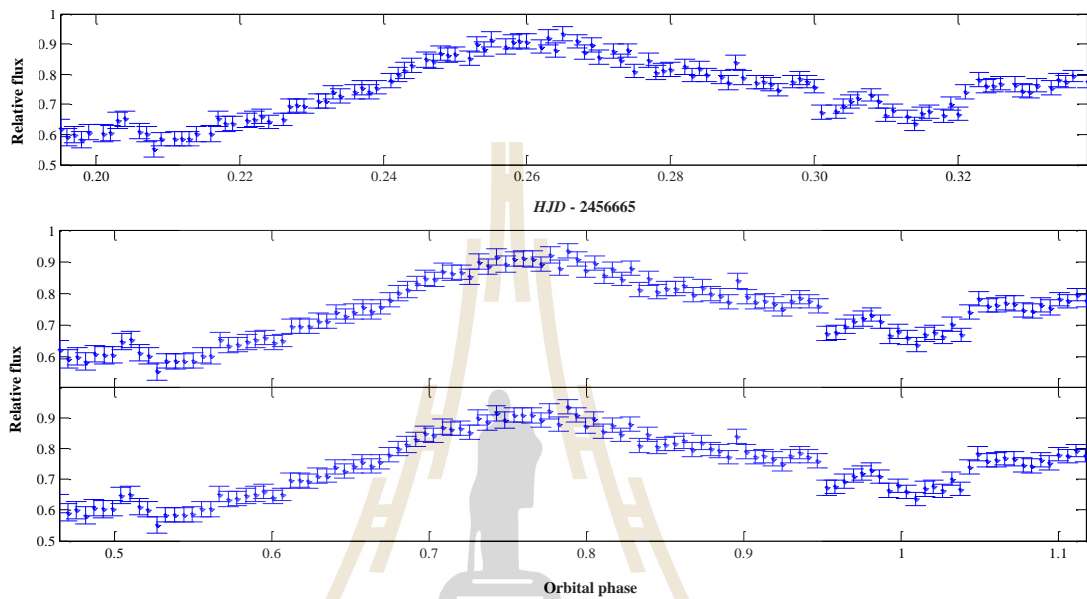


Figure 3.9 Top, light curve from observing night of 7th January 2014 by using a reference T_0 in HJD 2456665.3118 which the x axis is HJD and the y axis is relative flux. Middle, the light curve from observing night of 7th January 2014 by using a reference T_0 in HJD 2456665.3118 which the x axis is orbital phase and the y axis is relative flux. Bottom, light curve from observing night of 7th January 2014 by using a reference T_0 in HJD 2453387.7552404 from parson et al. (2013) which the x axis is orbital phase and the y axis is relative flux.

3.4.1.1 Effective temperature of stars

According to Parson et al. 2013, the main-sequence spectral type is M2. The effective temperature range between the main-sequence spectral type M5 and

M0 is 3170 – 3840 K (Zombeck, 2007). So in the model, the effective temperature is increased by 50 K in the range 3170 – 3840 K until we get the best value by consider the reduce Chi-square for the main-sequence star.

3.4.1.2 Mass ratio of the system

SDSS J0745 + 2631 show very large ellipsoidal modulation, implying that the main-sequence star almost fill its Roche lobe and the system has a high inclination (Parson et al., 2013). Since the Roche lobe's size depends on the mass ratio, for BM 3.0 modeling, the size of main-sequence is set filling its Roche lobe and varying the mass ratio of the system until the ingress and the egress time of model's eclipsing are well fit. The mass ratio (q) ~ 0.350 which the inclination of the system 90° for BM 3.0.

3.4.1.3 Inclination

The inclination of the system can be analyzed by considering the shape of the eclipse. Especially, the slope of the ingress and the egress time can tell us about the inclination of the system. When the inclination of system is 90° , it mean that the light curve in the ingress and egress time are almost a vertical line. If the inclination of system is less than 90° mean that the light curve in the ingress and egress time are incline. In Figure 3.11, the light curve shows a sharp decrease which imply a high inclination, where we test the range of inclination of $i = 75^\circ - 90^\circ$ by increment 0.5 until we get the best value by consider the reduce Chi-square.

3.4.1.4 Mass of main-sequence and white dwarf

The mass of white dwarf star can be derived by using the mass function. Since the radial velocity of the main-sequence star is 250 km/s (Parson et al., 2013), the main sequence's mass (M_{MS}) is 0.350 time of white dwarf's mass (M_{WD}),

($M_{MS} = 0.35M_{WD}$). The inclination of binary system is 90° and the orbital period is 0.21926 day. The mass function can be derived as

$$f(M_{WD}) = \frac{(M_{WD} \sin i)^3}{(M_{WD} + M_{MS})^2} = \frac{P_{obs}(K_{MS})^3}{2\pi G} \quad (3.2)$$

Using equation (3.2), we are able to determine the white dwarf's mass, $M_{WD} = 0.647M_\odot$ and main sequence's mass, $M_{MS} = 0.226M_\odot$.

3.4.1.5 Orbital separation

The Kepler 3rd law provided the orbital separation of two star. For circular orbits, the sum of the distance from the center of mass of each star to the center of mass of the system (CM) is defined as the semi major axis (a), $a = r_1 + r_2$ as seen in Figure 3.10. m_1 is the more massive star, m_2 is the less massive star, r_1 is the distance from m_1 to CM and r_2 is the distance from m_2 to CM. The time it takes to complete the orbit (the period) provides r_1 and r_2 by

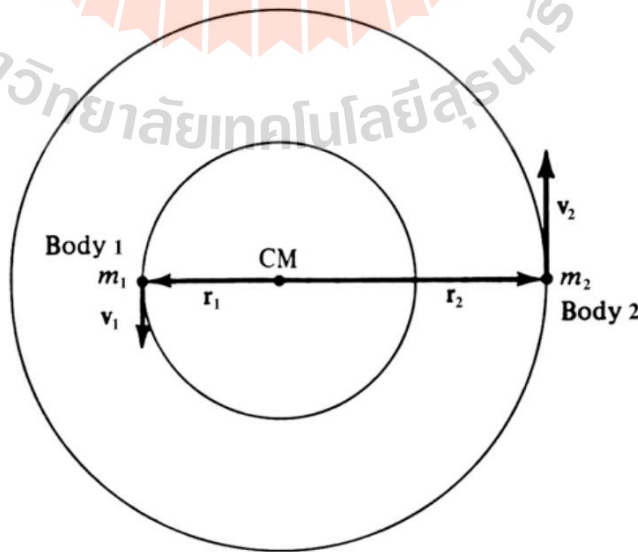


Figure 3.10 Diagram for circular orbits: CM marks the barycenter (center of mass).

$$P = \frac{2\pi r_1}{v_1} = \frac{2\pi r_2}{v_2} \quad (3.3)$$

where the orbital period P is 0.21926 days, radial velocity of white dwarf is $v_1 = 87.5$ km/s from the calculation and radial velocity of main sequence star is $v_2 = 250$ km/s from Parson et al. (2013). Thus, $r_1 = 753.8 \times 10^3$ km and $r_2 = 263.8 \times 10^3$ km from the calculation. So, the semi major axis, $a = r_1 + r_2 = 1017.6 \times 10^3$ km or in a solar radius is $a = 1.46R_{\odot}$.

3.4.1.6 Limb darkening

Limb darkening is the diminishing of the brightness of a star's surface as one looks away from its center, towards the edge of the disk (or limb). BM 3.0 uses the linear limb darkening law. This effect depends on the effective temperature of star and wavelength. From Al Naimiy (1978), the linear darkening coefficients are in the Table 3.3.

Table 3.3 Linear Limb Darkening Tables from Al Naimiy (1978).

| T_{eff} (K) | Limb darkening coefficient | | |
|---------------|----------------------------|------------------|------------------|
| | $\lambda=5000$ A | $\lambda=5500$ A | $\lambda=6000$ A |
| 14000 | 0.38 | 0.34 | 0.31 |
| 4000 | 0.97 | 0.88 | 0.81 |

3.4.1.7 Gravity Darkening Exponent

The surface flux is proportional to the value of the gravitational

acceleration (g) (Von Zeipel, 1924). For the BM 3.0, the Gravity Brightening Exponent α is 1.00 for radiative stars (the effective temperature higher than 7200 K) and is 0.32 for convective stars (the effective temperature less than 7200 K) (Lucy, 1967).

3.4.1.8 Reflection effect

When the radiation from one star strikes the surface of the other, its energy will heat up the receiving surface. For radiative stars (the effective temperature higher than 7200 K) the albedo effect will be approximately to be 1.00 and convective stars (the effective temperature less than 7200 K) the albedo will be approximately 0.50 (Rucinski, 1969).

3.4.1.9 Stellar spot

The BM 3.0 can provided a model with hot and/or cool spots on the stars. The input parameters are the spot colatitude, the spot longitude, the spot radius and the effective temperature factor. The spot effective temperature factor is defined as the percentage hotter or cooler that the spot effective temperature is relative to the local effective temperature. The spot radius is defined as the approximately circular radius in degrees of the spot region centered at the colatitude and longitude coordinates. The spot colatitude is the position angle (in degrees) of the center of the spot starting from the upper pole of a star measured along a meridian line towards the lower pole. The spot longitude is the position of a star spot measured along the equator of a star in degrees starting at the sub stellar point (the point directly in line with its companion along the line connecting the two mass centers) as 0° and going counterclockwise as seen from the positive end of the angular momentum vector to 360° .

SDSS J0745 +2631 needs a spot effect on the model to fit the light curve. At orbital phase around 0.5, the light level is lower than orbital phase 1.0 (see

Figure 3.11). So in term of modeling with BM 3.0, the spot effects were adapted which the large cold spot at co-latitude around 0° co-longitude 90° .

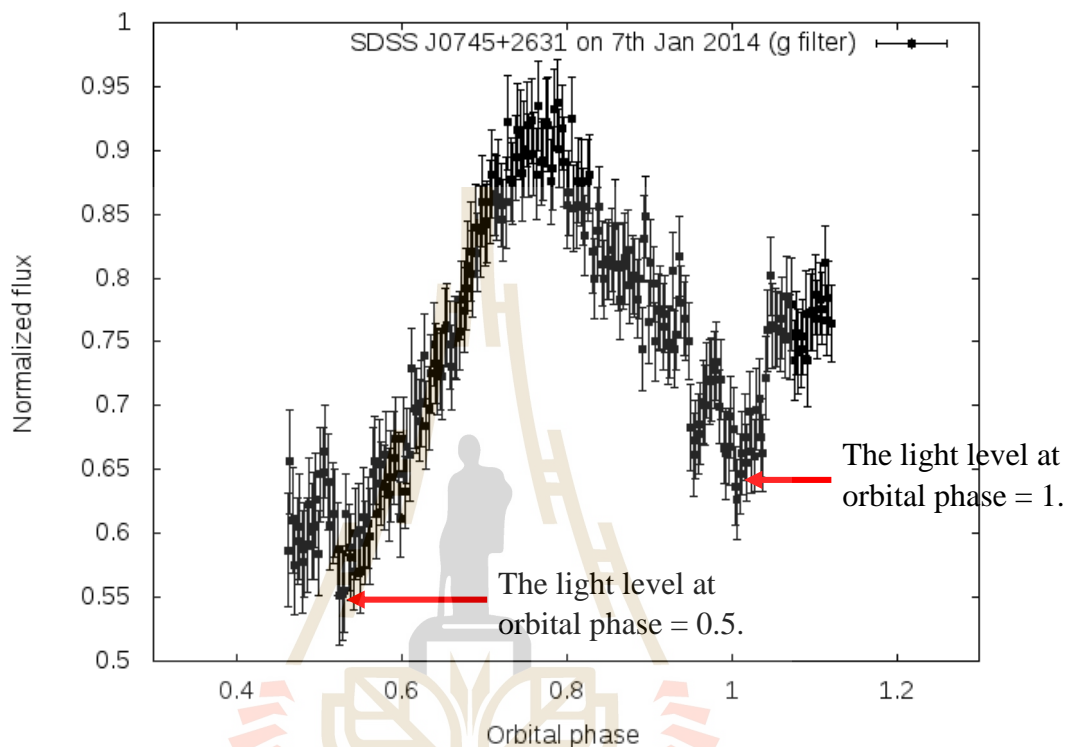


Figure 3.11 the light curve of SDSS J0745 +2631 from observational night 7th January 2014. The orbital phase at 0.5 show a level light curve lower than phase 1.0.

3.4.2 JKTEBOP code

JKTEBOP is the program to model the light curve of detached binary star. It is written in FORTRAN 77 by John Southworth et al. (2004). The JKTEBOP code reads specific format text file as an input and it also writes the output in text format. The light curve has to be prepared because it will be taken as one of the input. The input file need initial parameters such as sum of fractional radii, the mass ratio of the system and the surface brightness ratio, orbital inclination of the system. The JKTEBOP can iteratively

adjust the model until it give the best fit model.

The output of parameters from BM 3.0 were used as the initial parameters for JKTEBOP such as the mass ratio of the system = 0.350, fixed the inclination of the binary system ($i = 90^\circ$, fixed). The initial parameters for JKTEBOP are shown in the Table 3.4. The JKTEBOP gives an output file which contain the output parameters after iterative calculation for the best parameters as seen in Table 3.5, the best-fitting model light curve.

Table 3.4 The initial parameter of JKTEBOP for SDSS J0745 +2631 from observation night 7th January 2014. The input values are written in the two leftmost columns, while the description of those two columns are written on the right sides.

| 3 | 5 | Task to do (from 2 to 9) | Integ. ring size (deg) |
|-------|--------|----------------------------|--------------------------|
| 0.295 | 43.741 | Sum of the radii | Ratio of the radii |
| 90 | 0.35 | Orbital inclination (deg) | Mass ratio of system |
| 0.0 | 0.0 | ecosw or eccentricity | esinw or periastron long |
| 1.0 | 0.5 | Gravity darkening (star A) | Grav darkening (star B) |
| 0.006 | 0 | Surface brightness ratio | Amount of third light |
| sqrt | lin | LD law type for star A | LD law type for star B |
| 0.0 | 0.0 | LD star A (linear coeff) | LD star B (linear coeff) |
| 0.723 | 0.191 | LD star A (nonlin coeff) | LD star B (nonlin coeff) |
| 1.0 | 0.32 | Reflection effect star A | Reflection effect star B |

Table 3.4 The initial parameter of JKTEBOP for SDSS J0745 +2631 from observation night 7th January 2014. The input values are written in the two leftmost columns, while the description of those two columns are written on the right sides (Continued).

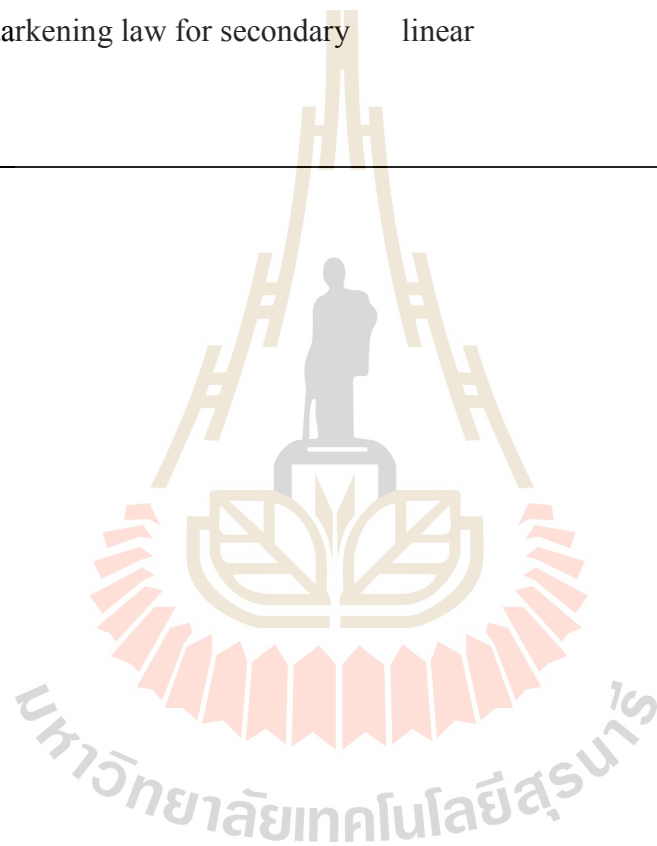
| | | | |
|--------------|-----|--|--------------------------|
| 0.0 | 0.4 | Phase of primary eclipse | Light scale factor (mag) |
| 0.2192638284 | | Orbital period of eclipsing binary system (days) | |
| 56664.805364 | | Reference time of primary minimum (<i>HJD</i>) | |
| 0 | 1 | Adjust RADII SUM | Adjust RADII RATIO |
| 0 | 0 | Adjust INCLINATION | Adjust MASSRATIO |
| 0 | 0 | Adjust ECOSW-or-E | Adjust ESINW-or-OMEGA |
| 0 | 0 | Adjust GRAVDARK1 | Adjust GRAVDARK2 |
| 1 | 0 | Adjust SURFBRIGHT2 | Adjust THIRDLIGHT |
| 0 | 0 | Adjust LD-LIN star A | Adjust LD-LIN star B |
| 0 | 0 | Adjust LD-NONLIN A | Adjust LD-NONLIN B |
| 1 | 1 | Adjust REFLECTION A | Adjust REFLECTION B |
| 1 | 1 | Adjust PHASESHIFT | Adjust SCALE FACTOR |
| 0 | 1 | Adjust PERIOD | Adjust T(pri.ecl.) |

Table 3.5 The final stellar and binary parameters for SDSS J0745 +2631 from observation night 7th January 2014 by using JKTEBOP code.

| | | |
|----|---------------------|---------------------------------|
| 1 | Surf. Bright. Ratio | 0.0066113071 +/- 0.0051643005 |
| 2 | Sum of frac radii | 0.2950000000 (fixed) |
| 3 | Ratio of the radii | 39.1023230007 +/- 15.5229710254 |
| 4 | Limb darkening A1 | 0.0000000000 (fixed) |
| 5 | Limb darkening B1 | 0.0000000000 (fixed) |
| 6 | Orbit inclination | 90.0000000000 (fixed) |
| 7 | ecc * cos(omega) | 0.0000000000 (fixed) |
| 8 | ecc * sin(omega) | 0.0000000000 (fixed) |
| 9 | Grav darkening A | 1.0000000000 (fixed) |
| 10 | Grav darkening B | 2.3987994926 +/- 0.1689387186 |
| 11 | Reflected light A | 0.0000206381 (from geometry) |
| 12 | Reflected light B | -0.0763526721 +/- 0.0015055395 |
| 13 | Phot mass ratio | 0.3500000000 (fixed) |
| 14 | Third light (L3) | 0.0000000000 (fixed) |
| 15 | Phase correction | 0.0000000000 (fixed) |
| 16 | Light scale factor | 3.9567916712 +/- 0.0021190060 |
| 17 | Integration ring | 5.0000000000 (fixed) |
| 18 | Orbital period (P) | 0.21926383 (fixed) |

Table 3.5 The final stellar and binary parameters for SDSS J0745 +2631 from observation night 7th January 2014 by using JKTEBOP code (Continued).

| | | |
|----|--|-----------------------------------|
| 19 | Ephemeris time base | 56664.8059432006 +/- 0.0001607609 |
| 20 | Limb darkening A2 | 0.7230000000 (fixed) |
| 21 | Limb darkening law for primary star: | Square-root |
| 22 | Limb darkening law for secondary star: | linear |



CHAPTER IV

RESULT AND DISCUSSIONS

4.1 Light curve analysis

SDSS J0745+2631 was observed in three different filters, where we obtained almost complete orbit in g' and r' filters. Even though the light curve in KG5 filter did not covered a complete orbital phase but we can derive the light curve's trend from the orbital phase calculation for each observational date.

The light curves from IRAF are shown in Figure 4.1 for each date of observation (see Table 3.2 for details). The filter used for each observing night is indicated in the plots. The light curves in g' filter show a large ellipsoidal modulation and the eclipses are more prominent compared to other wavelengths. The filter g' shows a clear eclipse, the eclipse is shallow might be due to the white dwarf has a low temperature. In Figure 3.11, the ingress and egress time of eclipse is very short, this imply that the white dwarf is very small and the brightness is increased a little bit immediately after its decreased. The increasing of the light curve during the eclipse might cause by the flares of the main-sequence star which we can see obviously in g' filter. The large scattering in the light curve is caused by the unstable weather condition during the observations.

4.2 Time of mid-eclipse

The first step of finding the mid-eclipse in each observing night, we used the

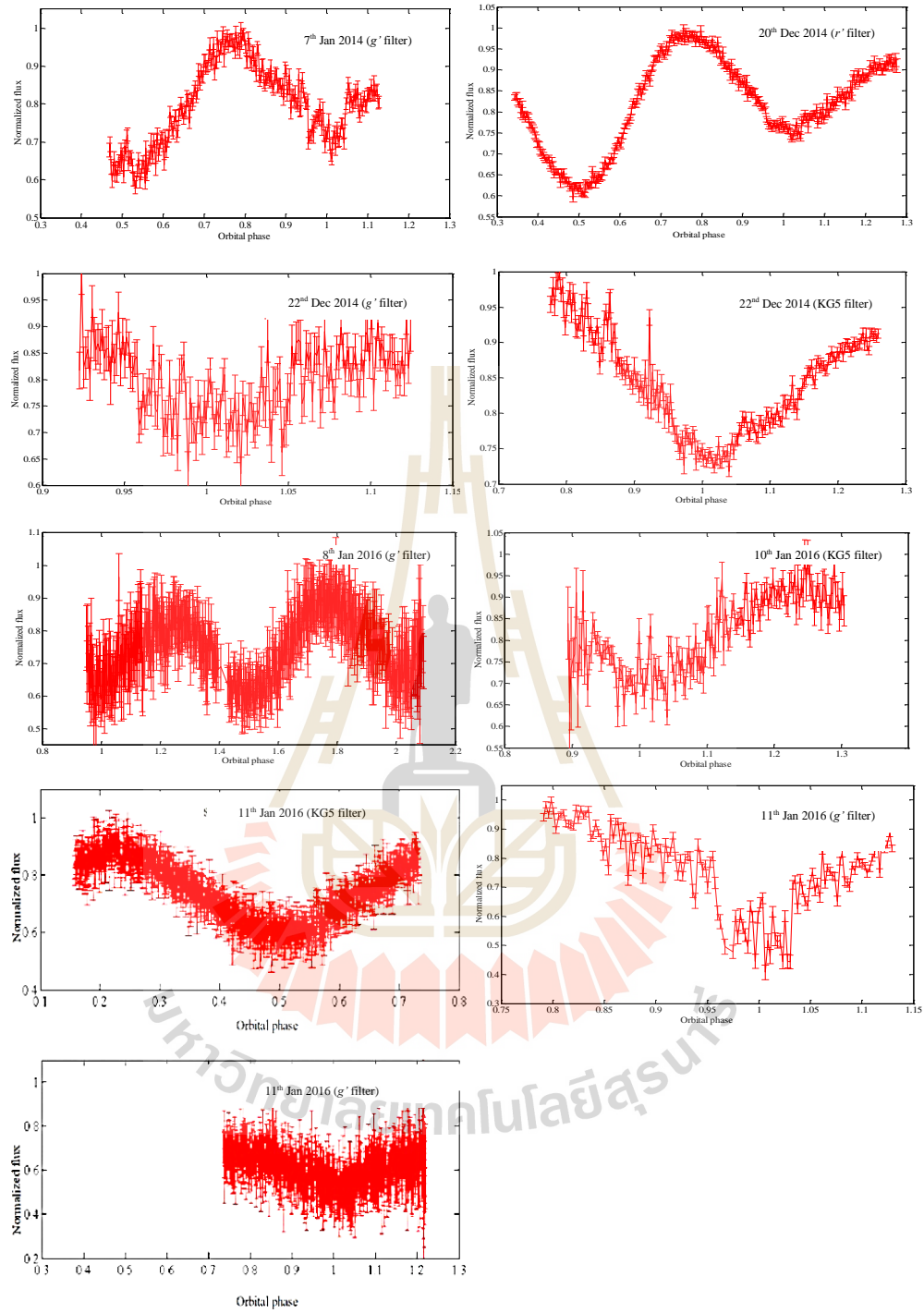


Figure 4.1 The light curves of SDSS J0745+2631 after bias subtraction and flat-fielding by using IRAF according to the method explained in previous chapter. The primary eclipse were shown clearly in g' filter on 7th January 2014 and 11th January 2016 but the others are quite difficult to confirm the eclipse.

ephemeris of $T_0(HJD) = 2453387.75524$ and the orbital period = 0.2192638284 days from Parson et al., 2013. The prediction of the light curve phases are shown in Figure 4.2. The light curves by using BM 3.0 are shown in Figure 4.3. We determine the guessing mid-eclipse by defined as the middle of time between the ingress and egress time of eclipsing. The mid-eclipse from the model by BM 3.0 were used to be the initial parameter for JKTEBOP code is shown in the Table 4.1

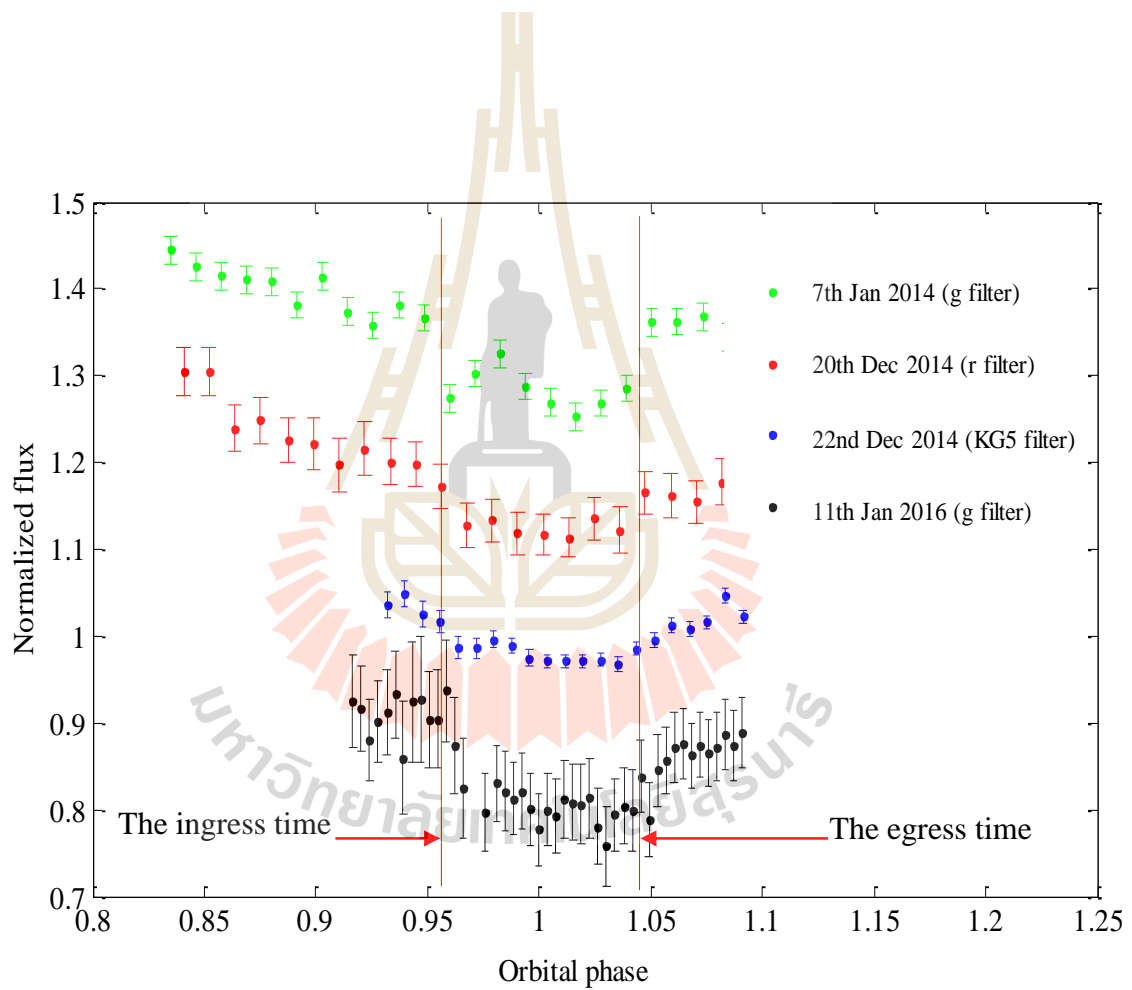


Figure 4.2 The light curves of SDSS J0745 +2631 in the range of the orbital phase 0.9 - 1.1 by using $T_0(HJD) = 2453387.75524$ and orbital period = 0.21926 days from Parson et al., 2013.

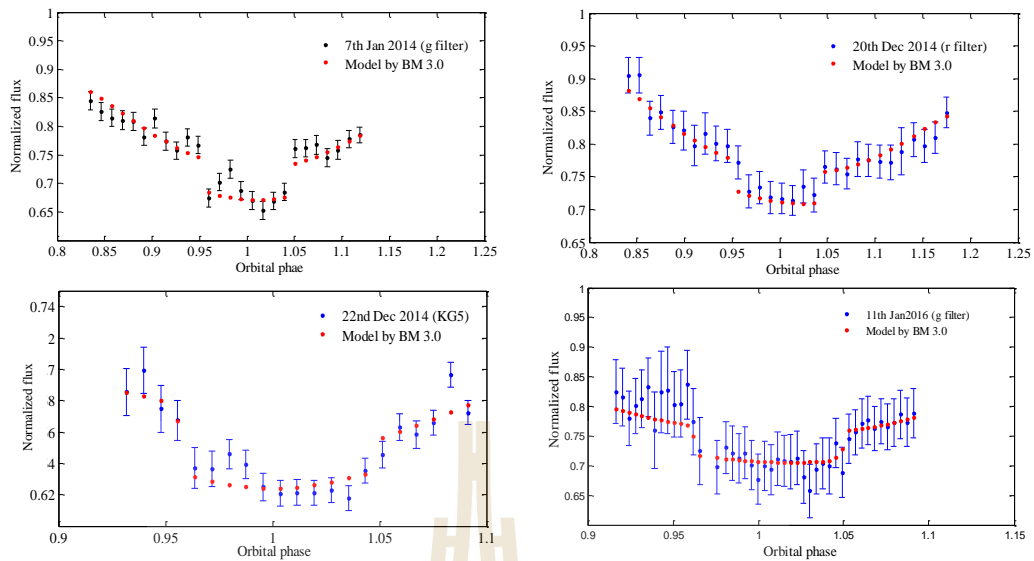


Figure 4.3 The light curves from observation and from BM 3.0 of 7th January 2014, 20th December 2014, 22nd December 2014 and 11th January 2016 from Top of left to right and bottom of left to right, respectively.

Table 4.1 The observed mid-eclipse time of SDSS J0745+2631 from the models by using BM 3.0.

| Observation night | Mid eclipse time (<i>HJD</i>) |
|---------------------------|---------------------------------|
| 7 th Jan2014 | 2456665.31082 |
| 20 th Dec 2014 | 2457012.40472 |
| 22 nd Dec 2014 | 2457014.15961 |
| 11 th Jan 2016 | 2457399.18862 |

The mid-eclipse timing can be calculated using the ephemeris and the $O - C$ method.

The observing mid-eclipse (O) of each light curve by using JKTEBOP code are shown in Table 4.2.

Table 4.2 The observed mid-eclipse time of SDSS J0745+2631 obtained from the output of JKTEBOP code.

| Observation night | Mid eclipse time (<i>HJD</i>) |
|---------------------------|---------------------------------|
| Parson et al. 2013 | 2453387.75524 |
| 7 th Jan 2014 | 2456665.31128 ± 0.00022 |
| 20 th Dec 2014 | 2457012.40499 ± 0.00093 |
| 22 nd Dec 2014 | 2457014.16403 ± 0.00022 |
| 11 th Jan 2016 | 2457399.18934 ± 0.00027 |

The mid-eclipse time from Parson et al., 2013 is used for a reference time (T_0). We can find the mid-eclipse from the observation by using JKTEBOP code. The mid-eclipse from calculation (C) of any observing nights were shown in Table 4.3.

Table 4.3 The predicted mid-eclipse time of SDSS J0745+2631 from calculation which $T_0(HJD) = 2453387.75524$ is used as a reference time and the orbital period = 0.21926 days from Parson et al., 2013.

| Observation night | Mid eclipse time (<i>HJD</i>) |
|---------------------------|---------------------------------|
| Parson et al. 2013 | 2453387.75524 |
| 7 th Jan 2014 | 2456665.31095 |
| 20 th Dec 2014 | 2457012.40559 |
| 22 nd Dec 2014 | 2457014.15970 |
| 11 th Jan 2016 | 2457399.18698 |

4.3 $O - C$ and ephemeris

To find the orbital period the linear ephemeris equation (2.17) was used and Table 4.4 shows the $O - C$ calculations for SDSS J0745 +2631 with orbital period (P) = 0.21926 days and the reference time $T_0(HJD) = 2453387.75524$ plot against epoch in Figure 4.4.

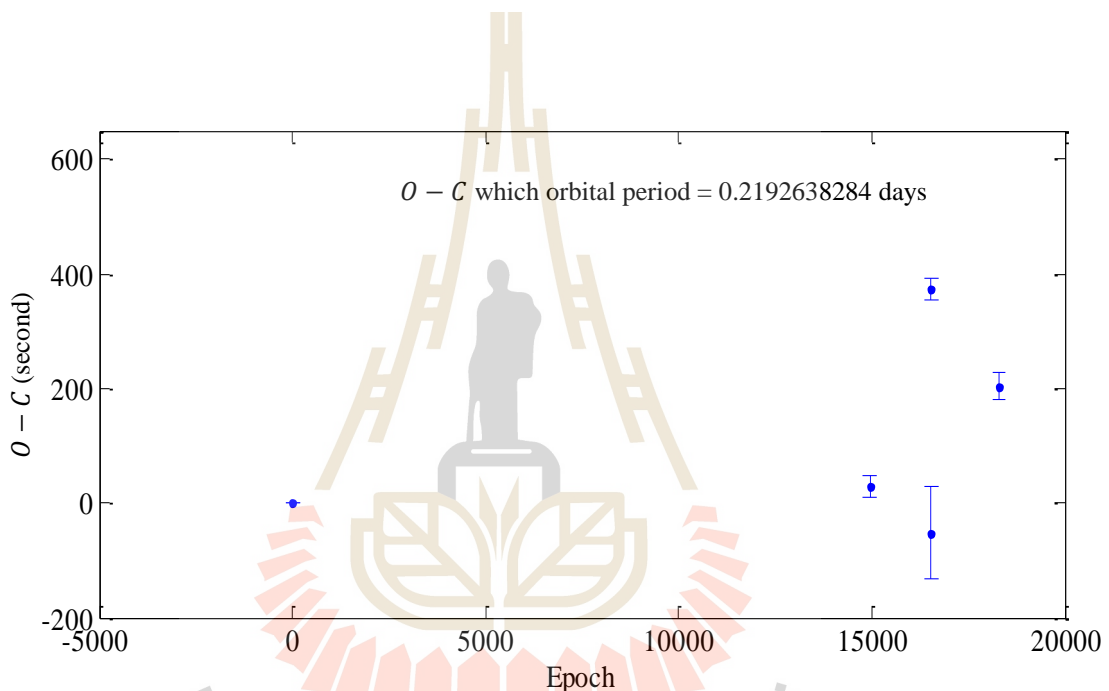


Figure 4.4 The $O - C$ diagram of SDSS J0745+2631. The calculation time mid-eclipse were used the orbital period 0.21926 days and the reference time $T_0(HJD) = 2453387.75524$.

The $O - C$ can tell us about the orbital period change if the $O - C$ is differed from zero then we can tell that the orbital period is changing. In the opposite way if the variation of $O - C$ is not different from zero then it means that the period of the system is quite stable. In Figure 4.4, we used the observed mid-eclipse at $T_0(HJD) =$

2453387.75524 from Parson et al., 2013 as the point of reference we found that the $O - C$ of 20th December 2014 and 22nd December 2014 scatter from zero value. However a change in the ephemeris is typically not detectable with two or few data points, such in our case. The cause of our $O - C$ scatter could be 1) the mid-eclipse time is not accurate due to a scatter of light curve and a shallow eclipse of system which made difficult to find the mid eclipse time, 2) the orbital period is changed with time, this can make the calculation mid-eclipse shifted from the observation, especially in long term of observation, the shift of mid-eclipse timing will be accumulated.

Table 4.4 The $O - C$ calculations with orbital period of 0.21926 days and the reference time $T_0(HJD) = 2453387.75524$ for the calculation of mid-eclipse.

| Orbital period (day) | Observation night | mid-eclipse time of observation (O) | mid-eclipse time of calculation (C) | $O - C$ (second) |
|-------------------------|---------------------------|--|--|-------------------------|
| 0.21926 | Parson et al. 2013 | 2453387.75524 | 2453387.75524 | 0.00000 |
| | 7 th Jan 2014 | 2456665.31128 ± 0.00022 | 2456665.31095 | 29.180 ± 19.008 |
| | 20 th Dec 2014 | 2457012.40499 ± 0.00093 | 2457012.40559 | -51.498 ± 80.352 |
| | 22 nd Dec 2014 | 2457014.16403 ± 0.00022 | 2457014.15970 | 374.469 ± 19.008 |
| | 11 th Jan 2016 | 2457399.18934 ± 0.00027 | 2457399.18698 | 203.430 ± 23.328 |

4.4 Light curve fitting

In term of modeling with JKTEBOP code and BM 3.0, we decided to use the light curves from the night of 7th January 2014, 20th December 2014, 22nd December 2014 and 11th January 2016. These light curves are good enough for modeling. We did the modeling first with BM 3.0 and then with JKTEBOP code. For JKTEBOP code, we can input parameters such as the masses, sizes, and effective temperatures of the stars in the system but it does not have spot parameter in the light curve modeling. The surface outline of the system is obtained using BM 3.0, as JKTEBOP code does not have a feature to draw the Roche configuration.

From the result, the main-sequence star is almost filling its Roche lobe, the temperature of the main-sequence is 3750 ± 250 K, mass ratio ($q = M_2/M_1$) is 0.350, and absolute radius is $0.450R_{\odot}$. We used the radial velocity data of the main-sequence from Parson et al. (2013).

4.4.1 Model with BM 3.0 program of SDSS J0745+2631

The light curve data of SDSS J0745+2631 from 4 observation nights were used for obtaining the model from BM 3.0 (Figure 4.5 and Figure 4.6). The initial parameters of BM 3.0 are derived in chapter 3, the size of the main-sequence star is fixed to fill its Roche lobe and the size will vary with mass ratio ($q = M_2/M_1$), which will help us to derive the radial velocity of the white dwarf. We also present the model with and without stellar spot.

As can be seen in Figure 4.5 and Figure 4.6, the model provides a better fitting to the data with spots included. The reduced Chi-square values for all models are given in table 4.5.

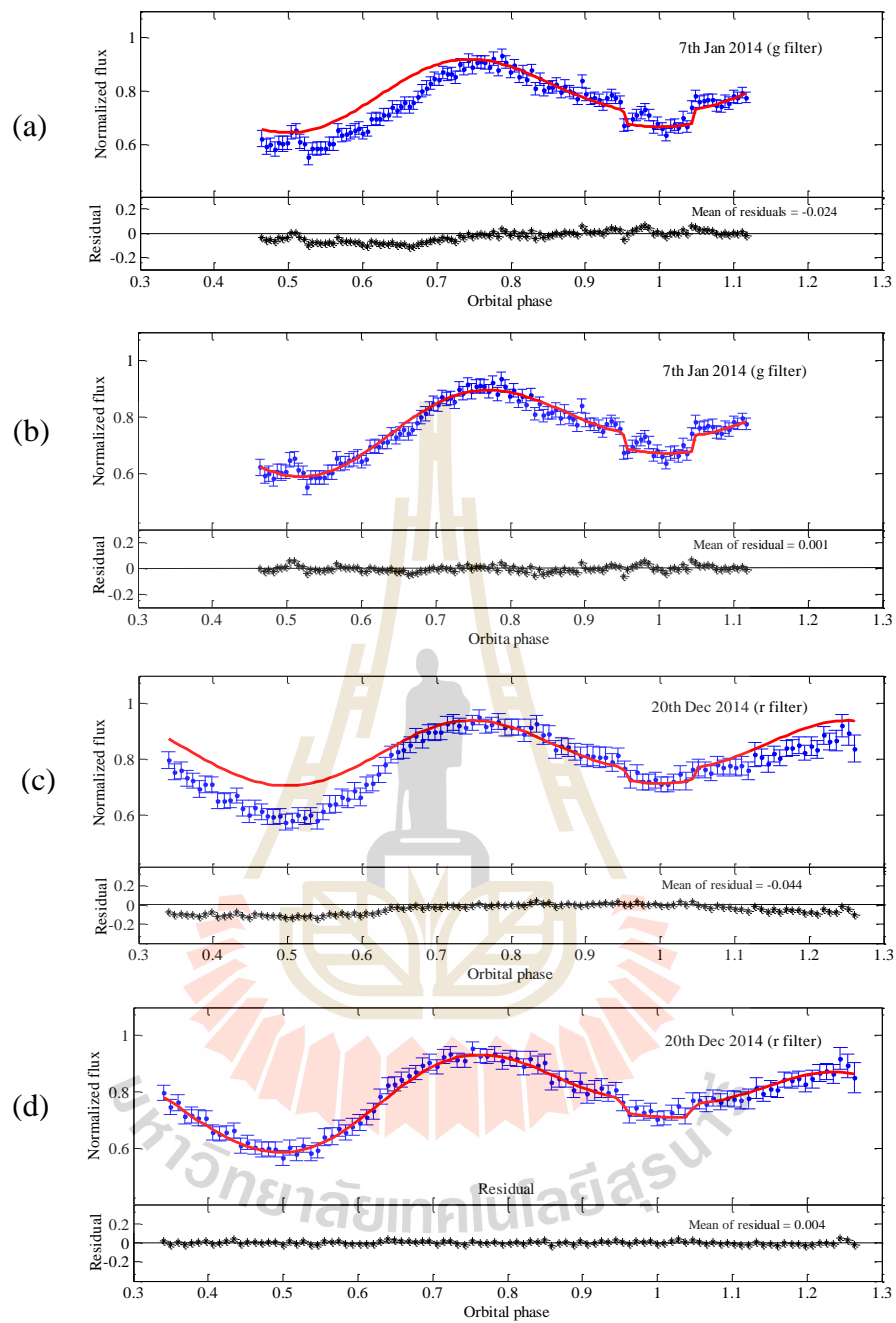


Figure 4.5 BM 3.0 model (a) without stellar spot and (b) with stellar spot for the data obtained on 7 January 2014. BM 3.0 model (c) without stellar spot and (d) with stellar spot for the data obtained on 20th December 2014. The observation data are plotted in blue points with error bars while the model is plotted in red line. The residuals are given in black points.

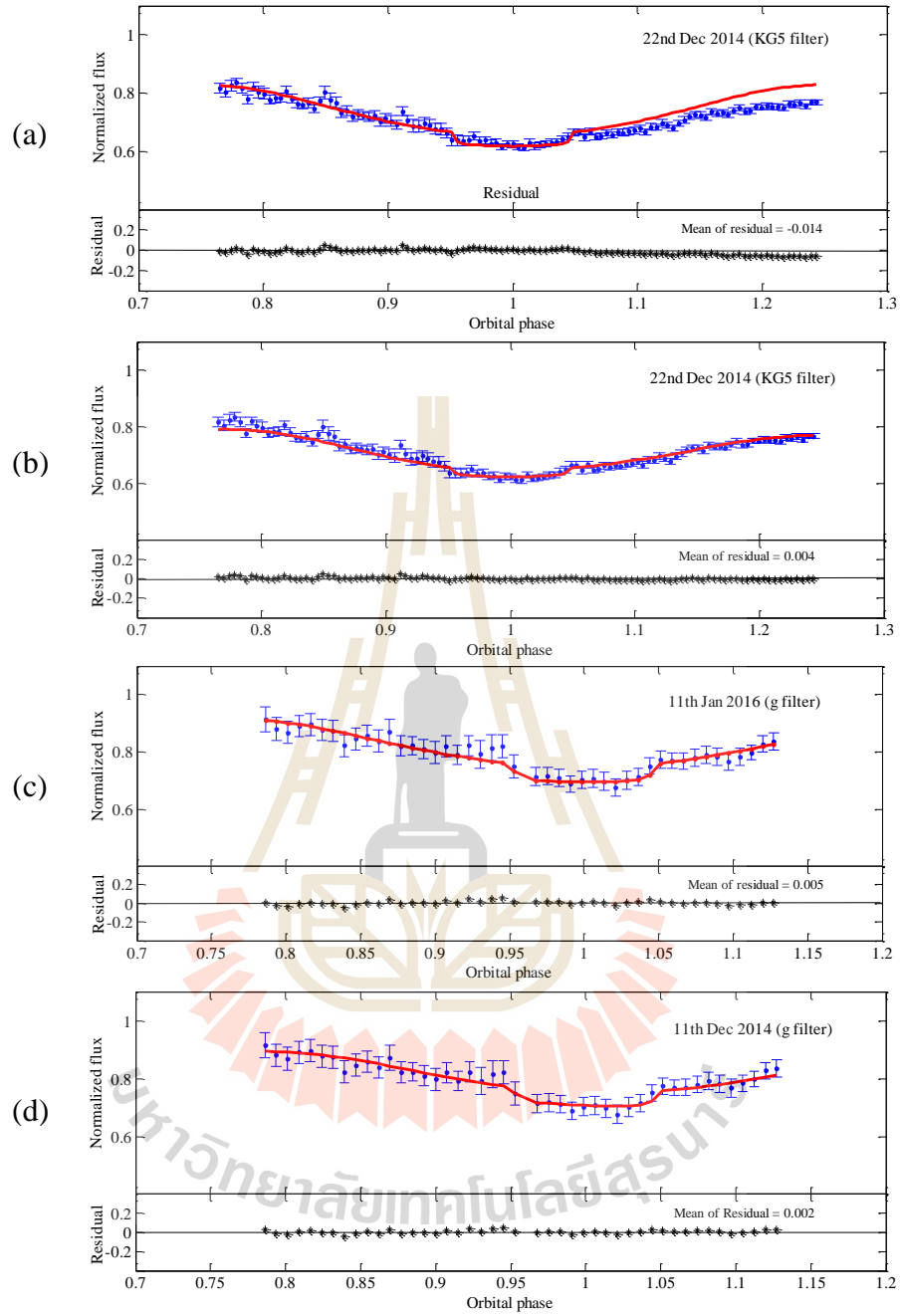


Figure 4.6 BM 3.0 model (a) without stellar spot and (b) with stellar spot for the data obtained on 22nd December 2014. BM 3.0 model (c) without stellar spot and (d) with stellar spot for the data obtained on 11th January 2016. The observation data are plotted in blue points with error bars while the model is plotted in red line. The residuals are given in black points.

Table 4.5 The reduced Chi-square value for models using BM 3.0.

| Observational night | The reduce Chi-square for the light curve data without spot | The reduce Chi-square for the light curve data with spots. |
|---------------------------|--|---|
| 7 th Jan 2014 | 4.549 | 1.016 |
| 20 th Dec 2014 | 5.248 | 0.369 |
| 22 nd Dec 2014 | 8.232 | 1.020 |
| 11 th Jan 2016 | 0.314 | 0.254 |

4.4.2 Model with JKTEBOP code of SDSS J0745+2631

JKTEBOP code cannot provide the Roche geometry and the spot like BM 3.0. However JKTEBOP code offers uncertainties for parameters which are not constrained/fixed. The initial parameters for the JKTEBOP code were separated into fixed and free parameters. In this works, we used the orbital period, orbital inclination, mass ratio as fixed parameters and the free unconstrained parameters are ephemeris time base as we mentioned in Chapter 3. JKTEBOP code will find the best fit to the light curve and give the new adjusted parameters of which the reduced Chi-square is used for the best fit of model. The model from JKTEBOP code are shown in Figure 4.7. The reduced Chi-square values of the light curve fitting with JKTEBOP code are presented in Table 4.6

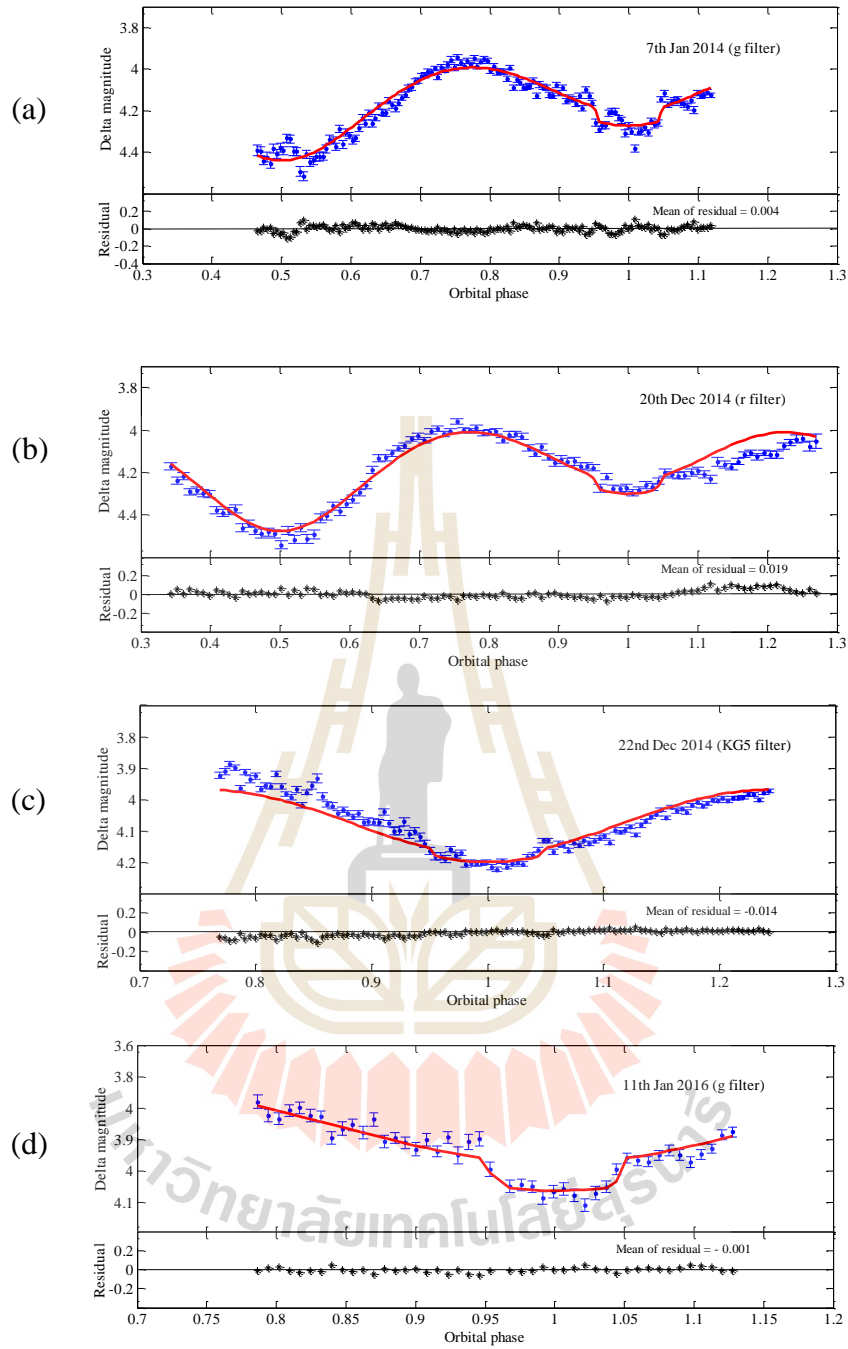


Figure 4.7 JKTEBOP models for the data obtained in the night of 7th January 2014 (a) and 20th December 2014 (b). JKTEBOP models for the data obtained in the night of 22nd December 2014 (c) and 11th January 2016 (d). The observation data are plotted in blue points with error bars while the model is plotted in red line. The residuals are given in black points.

Table 4.6 The Reduce Chi-square value for light curve data by using JKTEBOP.

| Observation night | reduce Chi square |
|---------------------------|-------------------|
| 7 th Jan 2014 | 5.892 |
| 20 th Dec 2014 | 7.836 |
| 22 nd Dec 2014 | 14.446 |
| 11 th Jan 2016 | 1.625 |

4.5 Stellar parameters

The light curve fitting of SDSS J0745+2631 with JKTEBOP code and BM 3.0 give final output parameters such as the mass ratio, radii of stars, orbital period, and inclination. The output parameters from the JKTEBOP code are shown below in Table 4.7. The model of SDSS J0745+2631 by using BM 3.0 is given the output parameters which shown in Table 4.8.

Table 4.7 Parameters of SDSS J0745+2631 from JKTEBOP code in 3 different filters and different observing nights.

| parameter | g' | r' | KG5 | g' |
|----------------------|--------------------------|---------------------------|---------------------------|---------------------------|
| | 7 th Jan 2014 | 20 th Dec 2014 | 22 nd Dec 2014 | 11 th Jan 2016 |
| Surf. Bright. ratio* | 0.005 | 0.008 | 0.004 | 0.005 |
| Sum of Frac. radii* | 0.295 | 0.295 | 0.295 | 0.295 |
| Ratio of the radii** | 39.102 | 43.741 | 40.571 | 39.102 |

Table 4.7 Parameters of SDSS J0745+2631 from JKTEBOP code in 3 different filters and different observing nights (Continued).

| parameter | g' | r' | KG5 | g' |
|-----------------------------------|--------------------------|---------------------------|---------------------------|---------------------------|
| | 7 th Jan 2014 | 20 th Dec 2014 | 22 nd Dec 2014 | 11 th Jan 2016 |
| Mass ratio* | 0.370 | 0.37 | 0.370 | 0.370 |
| Orbital inclination ($^\circ$)* | 86.75 | 86.75 | 86.75 | 86.75 |
| Orbital period (days)* | 0.21926 | 0.21926 | 0.21926 | 0.21926 |
| Frac. Radius of WD** | 0.007 | 0.007 | 0.007 | 0.007 |
| Frac. Radius of MS** | 0.288 | 0.288 | 0.288 | 0.288 |

* The parameters were fixed.

** The parameters were varies.

Table 4.8 Parameters of SDSS J0745+2631 from BM 3.0 with 3 different filters and different observational night.

| Parameters | g' | r' | KG5 | g' |
|----------------------------------|----------------------|-----------------------|-----------------------|-----------------------|
| | 7 th Jan. | 20 th Dec. | 22 nd Dec. | 11 st Jan. |
| | 2014 | 2014 | 2014 | 2016 |
| Mean radius WD (R_\odot) | 0.005 | 0.009 | 0.004 | 0.005 |
| Mean radius MS (R_\odot) | 0.439 | 0.425 | 0.432 | 0.439 |
| Effective wavelength (Å) | 4825 | 6561 | 5075. | 4825 |
| Orbital inclination ($^\circ$) | 85 | 90 | 87 | 85 |
| Effective Temperature of WD (K) | 14400 | 14925 | 14650 | 14400 |

Table 4.8 Parameters of SDSS J0745+2631 from BM 3.0 with 3 different filters and different observational night (Continued).

| Parameters | g' 7 th Jan. 2014 | r' 20 th Dec. 2014 | KG5 22 nd Dec. 2014 | g' 11 st Jan. 2016 |
|---------------------------------|--------------------------------------|---------------------------------------|--------------------------------------|---------------------------------------|
| Effective Temperature of MS (K) | 3750 | 3750 | 3750 | 3750 |
| Mass ratio | 0.370 | 0.350 | 0.390 | 0.370 |
| Mass of WD (M_{\odot}) | 0.657 | 0.649 | 0.652 | 0.657 |
| Mass of MS (M_{\odot}) | 0.230 | 0.227 | 0.228 | 0.230 |
| Semi-major axis (R_{\odot}) | 1.462 | 1.462 | 1.462 | 1.462 |
| Orbital period (days) | 0.21926 | 0.21926 | 0.21926 | 0.21926 |
| Temp Factor of Spot 1 on MS * | 0.700 | 0.700 | 0.700 | 0.700 |
| Size of Spot 1 on MS ** | 20 | 25 | 20 | 20 |
| Latitude of Spot 1 on MS *** | 90 | 90 | 90 | 90 |
| Longitude of Spot 1 on MS **** | 350 | 355 | 350 | 350 |
| Temp Factor of Spot 2 on MS* | 0.90 | 0.70 | 0.60 | 0.90 |
| Size of Spot 2 on MS ** | 15 | 14 | 13 | 15 |
| Latitude of Spot 2 on MS *** | 90 | 90 | 90 | 90 |
| Longitude of Spot 2 on MS **** | 100 | 100 | 100 | 100 |
| Luminosity of WD without spots | 0.060 | 0.050 | 0.046 | 0.060 |
| Luminosity of MS without spots | 0.940 | 0.950 | 0.954 | 0.940 |

Table 4.8 Parameters of SDSS J0745+2631 from BM 3.0 with 3 different filters and different observational night (Continued).

| Parameters | g' 7 th Jan. 2014 | r' 20 th Dec. 2014 | KG5 22 nd Dec. 2014 | g' 11 st Jan. 2016 |
|-----------------------------|--------------------------------------|---------------------------------------|--------------------------------------|---------------------------------------|
| Luminosity of WD with spots | 0.061 | 0.052 | 0.025 | 0.061 |
| Luminosity of MS with spots | 0.939 | 0.948 | 0.975 | 0.939 |

Note: Each star has a luminosity in a percent of a total luminosity.

- * Unit of Temp factor of spot is ratio of the spot temperature to the underlying effective temperature, of spots 1 and 2.
- ** Size of spot as the fractional measure of the amount that each star fills its respective Roche Lobe.
- *** Latitudes of spot. The North Pole is at a latitude of 0 degrees, the equator at 90 degrees, and the South Pole at 180 degrees.
- **** Longitudes of spot. The longitude is zero degrees at the inner Lagrange point, 90 degrees on the leading side, 180 degrees at the back end, and 270 degrees on the trailing side.

4.6 Discussions

SDSS J0745+2631 was one of the candidates of eclipsing binary where the light curve shows large ellipsoidal modulation, as presented by Parsons et al. 2013. Our first observation on 7th January 2014 was taken by using TNT with ULTRASPEC observed in g' filter. The data from this observation show a clear primary eclipse and confirm a

large ellipsoidal modulation outside the eclipse but we unable to detect the secondary eclipse. The ellipsoidal modulation observed in the light curve of SDSS J0745 is caused by the distortion of the low-mass main-sequence companion. The shallowness of the primary eclipse imply that the white dwarf has a low temperature. The cold spots were adapted in the model by BM 3.0 to fit the difference at orbital phase 0.5 which is lower than orbital phase 1.0.

4.6.1 Eclipse of SDSS J074548.63+263123.4

In this chapter, we obtained the light curves of J0745+2631 in g' , r' and KG5 filters. Among these light curves, only the data in g' filter which show a clear and visible eclipse. The flux of the main-sequence star dominates the overall flux at optical wavelengths. From the model the main-sequence star has a temperature (3750 ± 250 K) lower than the white dwarf (14594 ± 217 K). When the r' filter (redder wavelength) was used in observation, the signal from the main-sequence star contributes more than the white dwarf, which makes it more difficult to detect the primary eclipse. The opposite way, using the g' filter (bluer wavelength) gives more signal from the white dwarf but in our case the temperature of the white dwarf is low and cause a shallow eclipse.

4.6.2 Large ellipsoidal modulation and inclination

One of the interesting phenomena is the ellipsoidal modulation, this happened because of the distortion of the main-sequence star. The distortion of star shape can happen due to the evolutionary status of the star or due to the interaction with its companion in a binary. Parson et al., 2015 reported other PCEBs that show ellipsoidal modulation, SDSS J222918.95+185340.2 and SDSS J075015.11+494333.2. These system were identified as a close binaries by Drake et al. (2014). In Figure 4.8 (Parson et al., 2015), one peak is stranger than the other, this might be because the

O'Connell effect which is an asymmetry in the photometric in the light curve, this effect is often seen in PCEB with large Roche lobe filling and implying that there is the large spot on the main-sequence star.

SDSS J0745+2631 was one of candidates for eclipsing binary system with a shallow eclipse (Parson et al., 2013), the large ellipsoidal modulation and light curve look like SDSS J075015.11+494333.2 and SDSS J222918.95+185340.2. Even though these two light curves are not showed any obvious eclipse features. Figure 4.9 shows a geometry model of SDSS J0745+2631 obtained from BM 3.0 and Figure 4.10 shows the Roche surface of SDSS J0745+2631. We see that the main-sequence is almost filling its Roche lobe, so the influence of the main-sequence plays an important role in the light curve of this system. From light curves, our model the eclipse profile allow us to determine the system inclination angle i . The width of the primary eclipse not only had the effect with the size of stars but also the inclination of the binary system. A change in radii can be exactly compensated by a change in inclination (Ritter and Schroeder, 1979) as shown in Figure 4.11

For SDSS J0745+2631, the eclipse timing is about 28 minutes. This imply that the size of the white dwarf very small compared with the size of the main-sequence star. The magnitude variation of a shallow eclipse (~ 0.08 mags) is less than the magnitude variation of outside the eclipse (~ 0.45 mags), this imply that the white dwarf has a low effective temperature, the main-sequence almost fill the Roche lobe and the inclination of the binary system is very high, where we test the range of inclination of system, cover $i = 75^\circ - 90^\circ$. This approach allows us to determine the range of possible mass ratio, $q = \sim 0.35 - 0.39$. This given the most variation of light curve since the star fill the Roche lobe. Normally, during primary eclipse ($\phi = 1.0$) the light curve will reach

its lowest brightness but in J0745+2631, the light curve shows the lowest brightness at the orbital phase $\phi = 0.5$. To explain this phenomenon, we have applied the spot effect on the main-sequence star, where our models give better fit to the observation data.

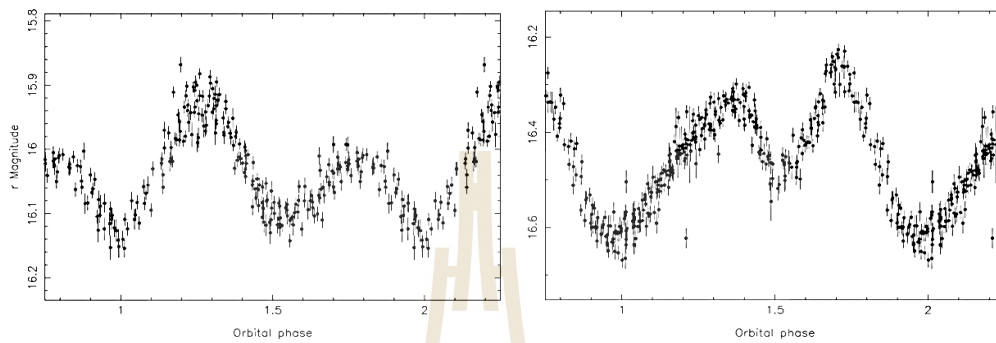


Figure 4.8 CSS light curves of SDSS J075015.11+494333.2 (left) and SDSS J222918.95+185340.2 (right). These show a variation of light curve similar to ellipsoidal modulation and light curves show clearly that one peak of them is stranger than the other, this might be cause of the O'Connell effect (adopted from Parsons et al. (2015)).

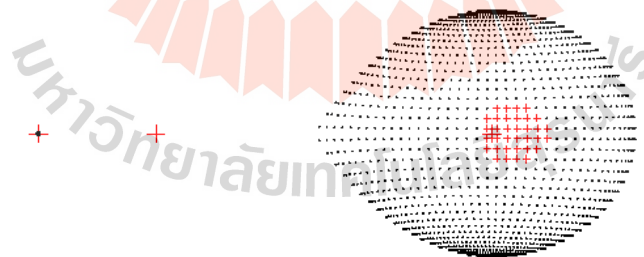


Figure 4.9 A geometry model at orbital phase 0.25 of SDSS J0745+2631 which inclination of the system 90 degree, the mass ratio 0.350, two red crosses are the center of mass of white dwarf and the binary system, the distortion shape star is the main-sequence star with the red region is spot.

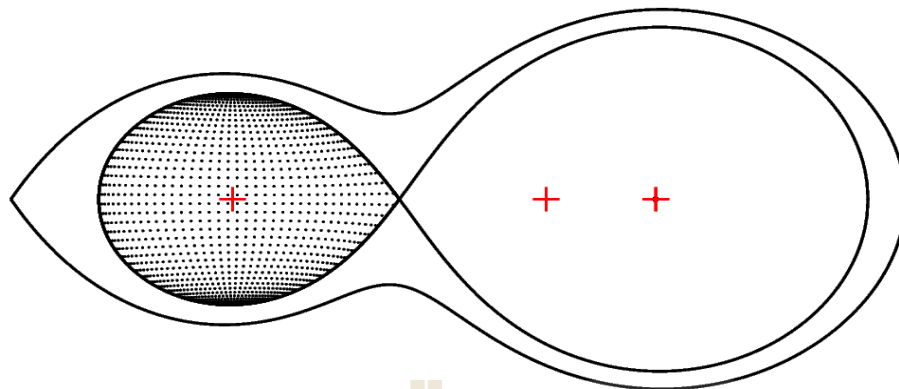


Figure 4.10 A surface outline of SDSS J0745+2631 inclination 90° , the mass ratio 0.350. The two solid lines are the inner and outer Roche lobe surrounding each star. Three red crosses are the center of mass for the main-sequence, the system and the white dwarf, respectively.

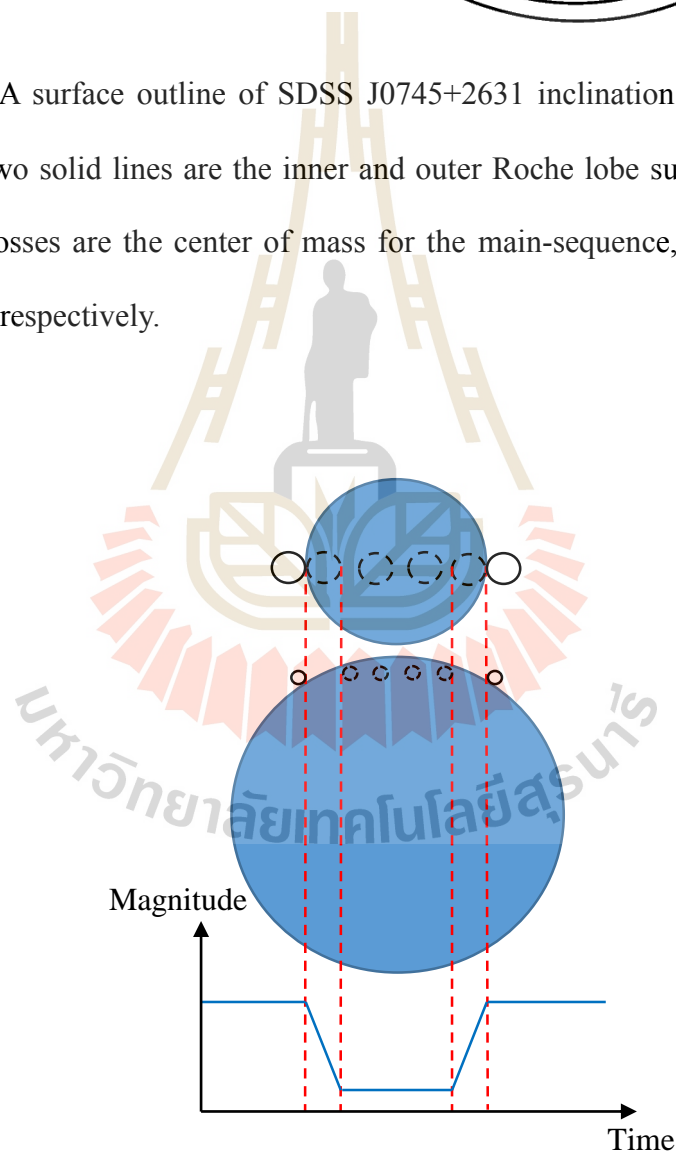


Figure 4.11 A Geometry of a primary eclipse which change a radii of stars can be exactly compensated by a change in inclination angle i .

4.6.3 Stellar parameters of SDSS J0745+2631

The luminosity of the star is the main parameter to help to investigate other parameters. Typically stellar luminosity are presented with the size and the effective temperature of a black body

$$L = \sigma A T_{eff}^4$$

where L is the luminosity in unit watt (W). σ is the Stefan–Boltzmann constant, with a value of $5.670367 \times 10^{-8} \text{ W m}^{-2} \text{ K}^{-4}$. A is a surface area of the star with unit meter square (m^2). We see that the light curves is affected by the main-sequence star although its effective temperature is lower than the effective temperature of the white dwarf, in this case can tell us that white dwarf's size is very compact. We cannot derive the effective temperature directly using JKTEBOP, but we can obtain the effective temperature by using the relation between the surface brightness ratios. The surface brightness ratio is

$$J = flux_{MS} / flux_{WD}$$

As

$$flux = \sigma T_{eff}^4$$

Then the surface brightness ratio is $\frac{flux_{MS}}{flux_{WD}} = \frac{\sigma T_{eff,MS}^4}{\sigma T_{eff,WD}^4}$

where $flux_{MS}$, $flux_{WD}$, $T_{eff,MS}$ and $T_{eff,WD}$ are flux of the main-sequence star, flux of the white dwarf, effective temperature of the main-sequence star and effective temperature of the white dwarf, respectively. The surface brightness ratio from JKTEBOP code is in range of 0.004 – 0.008. Thus the effective temperature of $T_{eff,WD}$ in range of $3.34T_{eff,MS} - 3.98T_{eff,MS}$. The main-sequence star is M2 star which has the effective temperature $3750 \pm 250 \text{ K}$, the effective temperature of white dwarf then should be in the range of 12525 K – 14925 K. From the model by using BM 3.0, the

effective temperature of white dwarf is 14594 ± 217 K. The effective temperature is one of the main determinant of eclipse depth, where the ratio of primary and secondary eclipse depths roughly equal to the ratio of effective temperatures to the fourth power, via the Stefan-Boltzmann law. From the model using BM 3.0, the luminosity of the main-sequence is greater than the luminosity of the white dwarf. The luminosity of main-sequence is 95 percent of total light and the luminosity of white dwarf is only 5 percent of total light. The light percentage of each star from the model is in agreement with the varying of light curve due to the shape of the main-sequence star which looks like a tear drop. The white dwarf has a mass over 3 times of the main-sequence star. From model with BM 3.0, most of the spots are located around facing sides of the main-sequence and cancelling the reflection effect. Normally, the outside eclipse light curve in a binary system reach its maximum at orbital phase = 0.25 and orbital phase = 0.75 with equal brightness. The case of SDSS J0745+2631 is a bit difference because of the O'Connell effect on the star. Star spots are common to occur on the surface of a star with deep convective envelope, such in the case of M-type star, but they can also be found on stars with high magnetic activity.

4.6.4 Orbital period of SDSS J074548.63+26312.4

The five data points of our $O - C$ diagram are scattered. Therefore, more observations are needed to confirm if there is any orbital period change because the five point of data are not enough.

4.6.5 Stellar spot on SDSS J0745 +2631

The adopted effective temperature of the main-sequence is 3750 ± 250 K, where the outer layer is a convective zone and energy is transported from hotter regions at the bottom to cooler regions above. This flowing of hot plasma creates the star

magnetic field. The star spot like the Sunspot typically has strong magnetic field. Thus it can redistribute heat within the star. From our model of SDSS J0745+2631 by using BM 3.0 the large cool spots on the main-sequence star located at the colatitude 0° which the surface of the star bulge out. This means that the distance from the center of main-sequence to its surface is longer and the temperature would be lower than any positions of star surfaces.

4.6.6 Reflection effect

SDSS J0745+2631 consists of the main-sequence star and the cool white dwarf with 14034 ± 480 K but the reflection effect for PCEBs contains a hot white dwarf similar to HS 1857+5144, $T_{WD} \approx 70000-100000$ K (Aungwerojwit, 2007). The reflection effect not only affect the effective temperature of white dwarf but also the orbital separation. The near contact binary system given a strong of reflection effect more than a detached binary system. For SDSS J0745+2631, the reflection effect is quite small due to a large of separation of two star and the effective temperature of white dwarf is low.

CHAPTER V

CONCLUSIONS

5.1 Conclusions

SDSS J0745+2631 is confirmed to be the eclipsing binary star. From the light curve shows clear eclipse feature as seen in g' filter with orbital period of 0.21926 days but we were unable to detect the eclipse in r' filter, it implies that the main-sequence is more dominating in the red wavelength. The mass of the white dwarf ($0.654 \pm 0.003M_{\odot}$) is nearly 3 times of the main-sequence mass ($0.229 \pm 0.001M_{\odot}$) and the mass ratio (M_{MS}/M_{WD}) = 0.37 ± 0.01 . The effective temperature of the white dwarf is 14594 ± 217 K and the effective temperature of the main-sequence is 3750 ± 250 K. The orbital separation of two star is $1.462R_{\odot}$. The reflection effect of this system is very small because of the effective temperature of the white dwarf and a large separation of two stars. Since the main-sequence has almost filled its Roche lobe, the shape is distorted and the light curve has large ellipsoidal modulation, which can be confirmed using the BM 3.0 model. The inclination of system $i = 87^{\circ} \pm 2^{\circ}$, the radius of the white dwarf is $0.008 \pm 0.002R_{\odot}$ and the radius of the main-sequence star is $0.427 \pm 0.006R_{\odot}$. The model shows the large cool spot on the co-longitude 90° of the main-sequence star which was derived using BM 3.0. This imply that the surface of the main-sequence star is convective, the flowing of hot plasma create the star magnetic field and the star spot. Table 5.1 shows the stellar and binary parameters of SDSS J0745 +2631 which was determined using BM 3.0 and JKTEBOP.

Table 5.1 The stellar and binary parameters of SDSS J0745 +2631 were obtained by using BM 3.0 and JKTEBOP code in SDSS g' filter.

| Parameters | BM 3.0 | JKTEBOP code |
|--|----------------------------|----------------------------|
| Mass Ratio (M_2/M_1) | 0.37 ± 0.01 | |
| The effective temperature of the white dwarf | 14594 ± 217 K | - |
| The effective temperature of the main-sequence | 3750 ± 250 K | - |
| The radius of the white dwarf | $0.006 \pm 0.002R_{\odot}$ | $0.010 \pm 0.002R_{\odot}$ |
| The radius of the main-sequence | $0.434 \pm 0.006R_{\odot}$ | $0.421 \pm 0.002R_{\odot}$ |
| The binary separation (a) | $1.46R_{\odot}$ | $1.46R_{\odot}$ |
| The inclination of system | $87^\circ \pm 2^\circ$ | 87° |
| The orbital period | 0.21926 days | 0.21926days |
| Mass of the main-sequence | $0.229 \pm 0.001M_{\odot}$ | - |
| Mass of the white dwarf | $0.654 \pm 0.003M_{\odot}$ | - |
| The reflection of the white dwarf | 1.000 | 0.000 |
| The reflection of the main-sequence | 0.500 | -0.076 ± 0.002 |
| The gravity darkening of the white dwarf | 1.000 | 1.000 |
| The gravity darkening of the main-sequence | 0.320 | 2.399 ± 0.169 |
| The limb darkening of the white dwarf | 0.400 | - |
| The limb darkening of the main-sequence | 0.600 | - |
| The spot on the main-sequence | 0.700 | - |
| Temp Factor of Spot 1 | 20 | - |

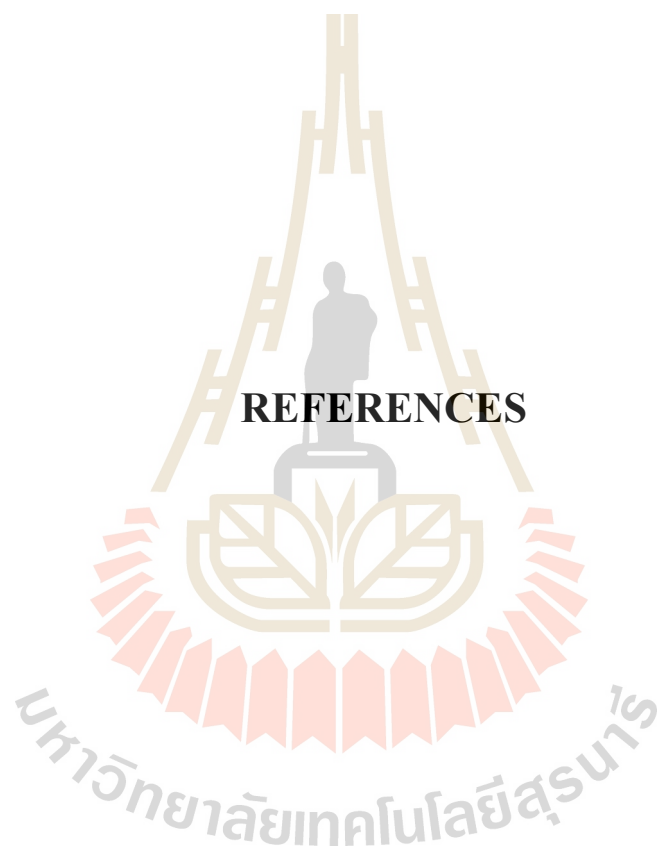
Table 5.1 The stellar and binary parameters of SDSS J0745 +2631 were obtained by using BM3 and JKTEBOP code in SDSS g' filter (Continued).

| Parameters | Binary Maker 3.0 | JKTEBOP code |
|-----------------------|------------------|--------------|
| Size of Spot 1 | 90 | - |
| Longitude of Spot 1 | 340 | - |
| Latitude of Spot 1 | 0.90 | - |
| Temp Factor of Spot 2 | 0.90 | - |
| Size of Spot 2 | 15 | - |
| Longitude of Spot 2 | 190 | - |
| Latitude of Spot 2 | 100 | - |

5.2 Future work

For this work, we understand the evolution of eclipsing binary which SDSS J0745 +2631 in post common envelope stage. However, the main-sequence star is expanded almost filling its Roche lobe and the outer layer is a convective zone with high magnetic activity. Although our data can detect the eclipse but they are not enough for the accurate of the $O - C$. Therefore, another photometric observation, are needed. As SDSS J0745 +2631 light curve shows a large ellipsoidal modulation, the spot effects were used in BM 3.0 model but JKETEBOP code cannot construct the model with spot effect. Thus, it might be work to try another programs for modeling the light curve with the spot effect and compares the result with our model.

REFERENCES



REFERENCES

- Al-Naimiy, H.M. (1978). Linearized limb-darkening coefficients for use in analysis of eclipsing binary light curves, **Astrophysics and Space Science**. 53: 181.
- Aungwerojwit, A. (2007). The properties of a spectroscopically selected sample of cataclysmic variables. **Ph.D. Thesis**. The University of Warwick.
- Benacquista, M.J. and Downing, J.M.B. (2013). Relativistic Binaries in Globular Clusters. **Living Review Relativity**. 16: 4.
- Carroll, B.W. and Ostlie, D.A. (2014). An Introduction to Modern Astrophysics, **Pearson Education Limited**.
- Dhillon, V.S., Marsh, T.R., Atkinson, D.C., Bezawada, N., Bours, M.C.P., Copperwheat, C.M., Gamble, T., Hardy, L.K., Hickman, R.D.H., Irawati, P., Ives, D.J., Kerry, P., Leckngam, A., Littlefair, S.P., McLay, S.A, O'Brien., K., Peacocke, P.T., Poshyachinda, S., Richichi, A., Soonthornthum, B. and Vick, A. (2014). Thai National Telescope. **Monthly Notices of the Royal Astronomical Society**. 444: 4009-4021.
- Drake, A.J., Graham, M.J., Djorgovski, S.J., Catelan, M., Mahabal, A.A., Torrealba, G., Garcia-Alvarez, D., Donalek, C., Prieto, J.L., Williams, R., Larson, S., Christensen, E., Belokurov, V., Koposov, S.E., Beshore, E., Boattini, A., Gibbs, A., Hill, R., Kowalski, R., Johnson, J. and Shelly, F. (2014). The Catalina Surveys Periodic Variable Star Catalog. **The Astrophysical Journal Supplement Series**. 213: 9.

- Fontaine, G., Brassard, P., Charpinet, S., Randall, S.K. and Van Groote, V. (2013). An overview of white dwarf stars. **EPJ Web of Conferences**. 43: 05001.
- Izzard, R.G., Hall, P.D., Tauris, T.M. and Tout, C.A. (2011). Common Envelope Evolution, **Proceedings IAU Symposium**. No. 283.
- Heintz, W. D. (1978). Double Stars, Dordrecht: D. **Reidel Publishing Company**
- Hilditch, R.W. (2001). An Introduction to Close Binary Stars. **Cambridge University Press**.
- Lucy, L.B. (1967). Gravity-Darkening for Stars with Convective Envelope. **Zeitschrift Fur Astrophysik**. 65: 89-92.
- Nelemans, G. and Tout, C.A. (2005). Reconstructing the evolution of white dwarf binaries: further evidence for an alternative algorithm for the outcome of the common-envelope phase in close binaries. **Monthly Notices of the Royal Astronomical Society**. 356: 753–764.
- Paczynski, B. (1976). Common Envelope Binaries. **Proceedings IAU Symposium**. No. 73.
- Parsons, S.G., Gansicke, B.T., Marsh, T.R., Drake A.J., Dhillon, V.S., Littlefair, S.P., Pyrzas, S., Rebassa-Mansergas, A. and Schreiber, M.R. (2013). Eclipsing post-common envelope binaries from the Catalina surveys. **Monthly Notices of the Royal Astronomical Society**. 429: 256-268.
- Parsons, S.G., Agurto-Gangas, C., Bours, M.C.P., Breedt, E., S.G., Gansicke, B.T., Marsh, T.R. Drake A.J., Dhillon, V.S., Littlefair, S.P., Pyrzas, S., Rebassa-Mansergas, A., Schreiber, M.R., Copperwheat C.M., Hardy L.K., Buisset C., Prasit P. and Ren, J.J. (2015). 14 new eclipsing white dwarf plus main-sequence binaries from the SDSS and Catalina surveys. **Monthly Notices of-**

the-Royal Astronomical Society. 449: 2194-2204.

Rucinski, S.M. (1969). The Photometric Proximity Effects in Close Binary Systems. I.

The Distortion of the Components and the Related Effects in Early Type Binaries. **Acta Astronomica.** 19: 12.

Sola, S. (2000). Reflection effect in PG 1336-018. **Baltic Astronomy.** 9: 197-204.

Southworth, J., Maxted, P.F.L. and Smalley, B. (2004). Eclipsing binaries in open clusters-II. V453 Cyg in NGC 6871. **Monthly Notices of the Royal Astronomical Society.** 351: 1277-1289.

Von Zeipel, E.H. (1924). The radiative equilibrium of a rotating system of gaseous masses. **Monthly Notices of the Royal Astronomical Society.** 84: 665–719.

Willems, B. and Kolb, U. (2004). Detached white dwarf main-sequence star binaries. **Astronomy and Astrophysics.** 419: 1057–1076.

Zombeck, M.V. (2007). Handbook of Space Astronomy and Astrophysics. **Cambridge University Press.**

CURRICULUM VITAE

Name: Mr. Niwat Hemha
Date of birth: 24th June 1990
Place of birth: Nakhon Phanom, Thailand
Personal address: 53, 10 Kutakai, Plapak, Nakhon Phanom 48160, Thailand
Nationality: Thai
E-mail: niwat_hemha@hotmail.com

Education

2009-2012 Mahasarakham University, Mahasarakham, Thailand
2012 – present Currently enrolling in Master degree majoring in Physics,
School of Physics, Institute of Science, Suranaree University of
Technology, Nakhon Ratchasima, Thailand

มหาวิทยาลัยเทคโนโลยีสุรนารี